



Studienabschlussarbeiten

Fakultät für Biologie

Makarov, Christine:

Analysis of brain structure in premature-born adults

Masterarbeit, Sommersemester 2021

Gutachter*in: Körte, Inga ; Wachinger, Christian

Fakultät für Biologie

Child and Adolescent Psychiatry at Ludwig-Maximilians-Universität München
Neurosciences

Ludwig-Maximilians-Universität München

<https://doi.org/10.5282/ubm/epub.91430>



Studienabschlussarbeiten

Fakultät für Biologie

Makarov, Christine:

Analysis of brain structure in premature-born adults

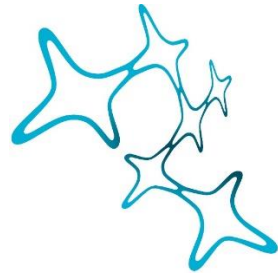
Masterarbeit, Sommersemester 2021

Gutachter*in: Körte, Inga ; Wachinger, Christian

Fakultät für Biologie

Child and Adolescent Psychiatry at Ludwig-Maximilians-Universität München
Neurosciences

Ludwig-Maximilians-Universität München



Graduate School of
Systemic Neurosciences
LMU Munich

Master's thesis in the study program MSc Neuroscience

Analysis of brain structure in premature-born adults

Christine Makarov née Grabosch

Matriculation number: 12170460

1st reviewer: Prof. Dr. Inga Körte

2nd reviewer: Prof. Dr. Christian Wachinger

Supervising Research Group: Child and Adolescent Psychiatry
at Ludwig-Maximilians-Universität München

Thesis dates (Start/ End): 26.04.2021-24.09.2021

Abstract

My master's thesis with the title "Analysis of brain structure in premature-born adults" is based on the discoveries of various developmental differences that have been found in premature-born individuals, both shortly after birth and in adults. However, it was not known to what extent these developmental differences are correlated and whether there might even be a causal relationship between structural differences and cognitive performance. To investigate these questions, MRI derived information on brain structure is combined in order to compute dependencies between different affected developmental processes. The analyses include statistical testing, correlation analysis as well as causal inference on a dataset consisting of 101 very preterm-born/ very low birth weight adults and 111 term-born control subjects. We found significant differences in very preterm-compared to term-born adults in multiple developmental processes, and these processes can be grouped by similarity into four main clusters. Furthermore, we found causal relationships between several developmental processes and cognitive performance. These findings pave the way for further research with the goal to improve risk prediction and the development of drug targets for preterm-born neonates.

Content

1	Introduction.....	- 6 -
1.1	Healthy development from week 20 to 40	- 6 -
1.2	Impairments in preterm birth	- 9 -
1.3	Treatment and restorative interventions in preterm birth.....	- 10 -
2	Related Work.....	- 12 -
3	Data	- 15 -
3.1	Participant information	- 15 -
3.2	Data acquisition.....	- 15 -
4	Methods	- 17 -
4.1	Correlation-Analysis	- 17 -
4.1.1	Categories for different developmental processes of tissue properties.....	- 17 -
4.1.2	Detection of areas with significant differences and effect sizes	- 17 -
4.1.3	Correlation Analysis of developmental disorders	- 18 -
4.1.4	Clustering.....	- 18 -
4.2	Causal Relationship Analysis	- 18 -
5	Results	- 22 -
5.1	Subquestion 1: What are the different developmental processes?	- 22 -
5.2	Subquestion 2: Which developmental processes have significant differences between VP/VLBW and FT individuals?.....	- 22 -
5.2.1	Visualisations of significantly different cortical and subcortical volumes	- 22 -
5.2.2	Visualisations of areas with significantly different cortical gyrification.....	- 25 -
5.2.3	White matter properties with significant differences.....	- 28 -
5.3	Subquestion 3: Which significant differences in developmental processes are correlated? ..	- 28 -
5.3.1	Correlation Matrices.....	- 28 -
5.3.2	Clusters in Correlation Matrices.....	- 30 -
5.3.3	Sparse PCA Analysis.....	- 32 -
5.3.4	Clusters in Participant Matrix.....	- 34 -
5.4	Subquestion 4: "What are the causal relationships between the MRI-derived measures that show significant differences between VP/VLBW and FT born individuals and IQ?"	- 36 -
6	Discussion	- 42 -
6.1	"Are there correlations between differences in developmental processes?"	- 42 -
6.2	"What are the causal relationships between the MRI-derived measures and IQ?"	- 43 -
6.3	Strengths and limitations	- 44 -
7	Conclusion	- 46 -
8	Publication bibliography.....	Fehler! Textmarke nicht definiert.

9	Appendix.....	- 54 -
9.1	P-values and effect sizes for significance analysis.....	- 54 -
9.2	Pair plot	- 61 -
9.3	Histogram for the distribution of IQ.....	- 62 -
9.4	Effect sizes of non-causally significant developmental processes	- 62 -

1 Introduction

Preterm birth describes birth before 37 weeks of gestation or with a birth weight below 2500g. The worldwide prevalence is approximately 11% of all births (Volpe 2019). In my thesis, I am focusing on very-preterm birth, which describes birth before 32 weeks of gestation or birth weight below 1500g, which occurs in about 1.4% of all births in the US. Multiple reasons can cause preterm birth, some happen spontaneously, others are induced because of medical reasons, for example, infections or chronic diseases of the mother. (Back et al. 2002; WHO 2021)

The problem with preterm birth, in general, is that with decreasing gestational age, survival rate decreases and incidences of neurological disabilities increase. These neurological disabilities include motor, cognitive, attentional, behavioural and socialisation disturbances (Volpe 2019). The disabilities are caused by short-term complications, on the one hand, for example, impairment of breathing, low blood pressure, temperature control, intraventricular haemorrhages, anaemia, and infections. On the other hand, long-term impairments associated with preterm birth include cerebral palsy, learning disabilities, retinopathy of prematurity, and chronic health issues (Mayo Clinic 2021a).

In my thesis, I am investigating the influence very preterm birth has on long-term brain development. The goal of my thesis is, firstly, to identify macroscopic developmental processes that are developing similarly and, secondly, to investigate which of these developmental processes are causes for cognitive impairment. Therefore, I will first look for correlations between impaired developmental processes in preterm birth and afterwards for causal relationships between structural measures and cognitive performance.

The overall goal of research on prematurely born adults is to analyse precisely which local structures are affected the most during development after preterm birth in order to make detailed observations of the impact of preterm birth on brain development. Ideally, the cellular components responsible for these structural changes can be identified more thoroughly in the future. Thus, it could pave the way for identifying targets for treating prematurely born children to avoid or counteract these structural changes during brain development. This, in turn, could lead to an improvement of the survival rate and at the same time to a reduction of the severeness of cognitive impairments as well as neurological diseases during the life course.

During brain development, all cell types and brain regions develop in their specific order and timeframe. However, premature birth leads to brain injuries that impair this healthy development. In the following paragraphs, I will explain healthy brain development and the impairments that occur in premature birth. I will mainly focus on the development between 20 and 40 weeks of gestation since this is the timeframe in which preterm birth can be located. During this time, especially cerebral white matter axons, subplate neurons, cerebral cortex, thalamus, and the basal ganglia will be of importance. However, not only neurons but also glial cells are affected, especially pre-oligodendrocytes (pre-OLs), microglia and astrocytes (Volpe 2019).

1.1 Healthy development from week 20 to 40

Gestational weeks (GW) 20 to 40 belong to the fetal period of development, which includes gyrification, neural development, and organisation and formation of synaptic connections (Stiles and Jernigan 2010). I will describe these processes in detail in the following section.

Neurogenesis. The proliferation of neurons begins in the embryonic period (GW 3-8) and is completed during the second half of gestation (Stiles and Jernigan 2010). Neurons proliferate in the ventricular zone and migrate to their respective destinations to form grey matter. One of these destinations is the neocortex, in which layering is a crucial part of development. This cortical layering is guided by radial glial cells to form the six layers. In contrast to this process called radial migration, a different type of

cell movement – tangential migration – also takes place. This type is mainly used by inhibitory interneurons and the large proportion of GABAergic cortical neurons that are differentiated late in development and start migrating tangentially through the white matter to the cortex between GW 24 and 40. The migration is completed six months after birth, after which the region of origin of the inhibitory interneurons will develop into the basal ganglia (Stiles and Jernigan 2010). The late migration makes them vulnerable to insults (Volpe 2019; Bystron et al. 2008; Letinic et al. 2002; Xu et al. 2011).

Cortical layering follows an inside-out principle, which means that the youngest neurons migrate to the most superficial layers. The only exceptions are the first neurons to proliferate. They form a preplate which is split into the marginal zone and the subplate. Afterwards, the first arriving neurons form the cortical plate, which is where layer six will be located in the further course of development. The marginal zone and the subplate are temporary structures that guide development but disappear in the late part of gestation. During fetal development, the marginal zone produces cells important for neuron-positioning, while the subplate neurons are responsible for establishing connections between the cortex and thalamus (see below). (Stiles and Jernigan 2010; Volpe 2019)

Subplate neurons. The subplate region starts to grow at around GW 20, and over the following weeks, neurons both from the cortex and thalamus make connections to subplate neurons. They then depart from the subplate layer to form the connections with their dedicated cells in cortical and subcortical areas, especially the basal forebrain. This mechanism is needed in order to collect axons that can not connect to their final targets because the respective cells have not differentiated yet. Also, the axons of subplate neurons promote differentiation, and once the correct cells are differentiated, they guide the input axons from the thalamus and cortex to their final position. After this task is completed, the subplate neurons die via apoptosis, and the subplate region starts to disperse in GW 36-40. Since the subplate region is especially active between GW 20 and GW 40, it is highly vulnerable to injuries that occur during this timeframe in preterm birth (Volpe 2019; Kostović and Jovanov-Milosević 2006; Kostović and Judas 2002; Bystron et al. 2008; Stiles and Jernigan 2010).

Gyrification. The cortical folding begins with the formation of gyri and sulci, particularly with the formation of the longitudinal fissure that acts as a separation of the two hemispheres. The development of the longitudinal fissure is complete at GW 22. Afterwards, primary, secondary and tertiary sulci form following a specific order until the formation is finished postnatally (Stiles and Jernigan 2010). The mechanisms of the folding process that generates highly similar folding patterns in all human brains are not fully understood, but hypotheses range from tangential expansion of the cortex to cortical factors, for example, axonal tension (Ronan et al. 2014).

Connectivity. After the neurons reach their position, they start to differentiate and form dendrites and axons (GW 20-24). Dendrites and axons are the structures that will allow for communication between cells via synapses, which are formed in GW 24-32. These connections form pathways in the white matter called fibre tracts. Axons can be isolated by myelin sheaths produced by oligodendrocytes (Stiles and Jernigan 2010; Volpe 2019). In the following paragraphs, I will go into more detail on axonal, dendritic, and synaptic development.

Axonal development. Axons develop until at least GW 37; from the thalamus, they reach the subplate at GW 20 and first connect to the cortex at GW 27. At this time, also commissural and corticocortical axons start to grow. The thalamus and the cortex are fully connected by GW 37. After GW 37, axons grow mainly inside the cortex and continue to do so during the first year after birth. Due to the timing of the axonal growth, axons are vulnerable to insults that occur in premature birth. (Volpe 2019; Haynes et al. 2005)

Dendritic development and further synaptogenesis. After the layering of the cortex is completed, the cortical surface has increased due to gyrification. At this point in time also GABAergic neurons have arrived in the upper cortical layers, dendrites, as well as axons, have grown, and synapses started to form. Because dendritic development is dependent on cortical activity, the connection between the subplate region and thalamus as well as commissural and corticocortical fibres is crucial for dendritic development. (Volpe 2019; Chen and Ghosh 2005; Sarnat et al. 2010)

Gliogenesis. Glial cells are the primary cell type in the brain besides neurons. They were believed to have mainly supportive roles, for example, maintaining the structure or regulating immune responses. Still, over the last years, more evidence has been found for glial cells to be actively involved in neuronal signalling (Cho et al. 2016). The main glial components involved in preterm birth are (pre-) oligodendrocytes, astrocytes, and microglia, whose functions during brain development I will explain in the following paragraphs.

Pre-oligodendrocytes. These cells are derived from oligodendrocyte progenitor cells, which proliferate at GW 20-24 and account for 90% of the lineage at the time of birth in premature-born children. At GW 24-32, many pre-oligodendrocytes can be found in the white matter, where they begin to ensheath axons at around GW 30 and are crucial for proper axonal and, therefore also cortical development. At term, 50% of the lineage is still made up of pre-OLs, while the other half consists of already further differentiated immature OLs. Fully differentiated oligodendrocytes will only occur later after birth in the brain and act as tissue-supporting cells (Volpe 2019; Back et al. 2001; Back et al. 2002; Reemst et al. 2016). Pre-OLs are highly vulnerable to hypoxia, ischemia and inflammation and therefore die when exposed to these insults. (Volpe 2019; Volpe et al. 2011)

Microglia. Microglia are part of the brain's immune system. Apart from that, they are involved in OL differentiation, axonal development, myelination, and synaptogenesis. Additionally, microglia can be participating in neuronal signalling via neurotransmitter receptors and the secretion of neuroactive molecules. These functions are regulated via proteins expressed in the microglia, which can also be responsible for the inflammatory activation of microglia. When activated in an immune response, microglia have the power to destroy cells via the generation of free radicals or cytokines. Microglia start populating the brain at GW 16-22 and migrate to white matter and cortex in GW 20-35. During this timeframe, an insult can activate the microglia and lead to cell destruction during critical developmental stages as well as problems with healthy development since these cells can no longer perform their intended tasks. (Volpe 2019; Schafer et al. 2012; Squarzoni et al. 2014; Reemst et al. 2016; Hickman et al. 2018; Hammond et al. 2018; Hammond et al. 2019; Billiards et al. 2006)

Astrocytes. Astrocytes are also crucial for development and are generated from GW 20-40. Their tasks in development include tissue support, axonal guidance, synaptogenesis, uptake of neurotransmitters in the synaptic cleft, and axonal survival. On the other hand, they can also sense synaptic activity and react to it in a tri-partite synapse. When in a reactive state, for example, after an injury, they undergo metabolic changes and can, among others, harm pre-OLs. (Volpe 2019; Reemst et al. 2016)

To summarise, brain development during the second half of gestation is a complex process with many interactions and dependencies that are highly vulnerable to injuries.

1.2 Impairments in preterm birth

Preterm birth means that especially the brain is not fully developed at the time of birth. The process of brain development involves complex and fine-tuned sequences of cellular events, which makes it highly vulnerable.

It is known that preterm birth leads to hypoxic-ischemic injuries in the brain, especially leading to cerebral white matter injury (WMI). This so-called "encephalopathy of prematurity" (Volpe 2009) includes dysmaturation of white matter as well as disturbances in neurons and axons. Furthermore, it involves activated microglia and astrocytes. This overall process leads to aberrant development and dysmaturation of pre-oligodendrocytes. Another pathway of injury could be directly via impact on cortical and subplate neurons and also via nutritional factors on cortical development. These processes combined lead to aberrant myelination and connectivity as well as neuron maturation. Consequently, cognitive and also motor performances can be impacted (Volpe 2019). WMI diagnosis is difficult since the identification of small lesions in MRI is complicated. However, children with no or minimal observed abnormality in the white matter also develop neurological disabilities. (Volpe 2019; Woodward et al. 2006; Anderson et al. 2017)

Overall findings in preterm birth include smaller regional volumes of cortex, WM, thalamus, and basal ganglia, as well as decreased fractional anisotropy (FA), decreased cortical surface area, less gyrification and impaired connectivity, especially thalamocortical connectivity (Volpe 2019). All of these observations have mainly been made at term-equivalent age, however, many changes persist into adulthood or even increase during further brain development (Volpe 2019; Zhang et al. 2015; Bataille et al. 2017; BANKER and LARROCHE 1962; Hedderich et al. 2020c). Therefore, in chapter 2, I will focus on findings in adults, while in this chapter, I will mainly explain the cellular processes that lead to impaired brain development.

The main driving force of encephalopathy of prematurity is cerebral white matter injury (WMI). WMI can be represented as periventricular leukomalacia (PVL) or diffuse white matter gliosis (DWMG). PVL causes focal necroses as well as diffuse lesions in white matter and includes the death of early differentiating pre-oligodendrocytes and astro- as well as microgliosis. The reason for these lesions is decreased cerebral blood flow (BANKER and LARROCHE 1962; Pierson et al. 2007; Okoshi et al. 2001; Shuman and Selednik 1980). The death of pre-oligodendrocytes has proliferation and failure of maturation of pre-oligodendrocytes as a consequence. This dysmaturation, in turn, causes hypomyelination of axons (Buser et al. 2012; Billiards et al. 2008; Haynes et al. 2003; Back 2017). DWMG without focal necroses show the same pattern of pre-oligodendrocyte dysmaturation and is the most common type of WMI in preterm born subjects. While the reason for the proliferation of more pre-oligodendrocytes is not yet understood, the problems with maturation are probably related to activation of astrocytes and microglia during development (see below) (Liddelow et al. 2017; Liddelow and Barres 2017; Back 2017; Volpe 2019).

To summarise these observations, in general, WMI follows a specific pattern of actions: First, an insult is responsible for cell death or injury, and consequently, pre-oligodendrocytes are proliferated but fail to mature. The severity of the injury is decisive for the seriousness of consequences, with mild injury targeting mainly pre-oligodendrocytes and more severe injury also acting on multiple other cell types and developmental processes. The exact primary causes are not identified, however, there are potential sequences that cause this dysmaturation, which I will now go into detail on. (Volpe 2019)

While activated astrocytes and microglia fail to perform their physiological tasks in axon development, they also actively harm pre-oligodendrocytes via the secretion of free radicals or cytokines. When pre-oligodendrocytes are damaged, cell death or process loss are consequences (Haynes et al. 2003; Billiards et al. 2008; Back 2017). As described above, after the cell death, pre-oligodendrocytes are

replenished, but the cells fail to mature and therefore are not able to produce myelin. Another possible way the pre-oligodendrocyte injury inflicts secondary problems is that while the pre-oligodendrocytes dysmature, they fail to ensheath the axons. Therefore, axon development is likely to be impaired. This ensheathment of axons by pre-OLs is also responsible for axonal growth in white matter and development of the cerebral cortex, both likely to be impacted by the injury to pre-oligodendrocytes. Consequently, volumes of cortex, thalamus and basal ganglia are likely to be smaller since the connecting projection fibres are injured. (Volpe 2019)

Another primary target of WMI is the thalamus, where neuron loss, gliosis, and axon degeneration are observed, and these injuries again contribute to further pre-oligodendrocyte dysmaturation (Pierson et al. 2007). On the other hand, impact on subplate neurons and consequent cell death can also be a cause for cortex and thalamus injury and subsequent pre-oligodendrocyte problems since subplate neurons are a population highly vulnerable to hypoxia-ischemia (Kostović and Judas 2002; McQuillen et al. 2003; Robinson et al. 2006; Kinney et al. 2012). Also, a deficit of late migrating GABAergic neurons was observed, which implies that this population could be injured during migration to the cortex. This would result in a loss of cortical neurons and, therefore, smaller volume, gyrification and connectivity in the cortex (Kinney et al. 2012; Robinson et al. 2006).

Apart from experiencing secondary injury, also primary injury to the grey matter is possible. Delayed microstructural development was observed via fractional anisotropy changes in grey matter, and therefore these changes are associated with impaired dendritic development (Volpe 2019). Additionally, this was reflected by impaired radial diffusion. The impact is hypothesised to be mainly via dysmaturation in the cortex, subplate neurons and caudate neurons, as observed in a sheep model. The impairments were found primarily in synapse formation and dendritic arborisation (Dean et al. 2013; McClendon et al. 2014).

Concluding, in preterm birth, pre-oligodendrocyte death leads to dysmaturation in grey and white matter, and a list of other injuries can be associated with pre-oligodendrocyte injuries, either as causes or consequences. Therefore, pre-oligodendrocytes could be a primary target when researching preterm birth and possible cellular implications, as well as for developing drugs or interventions that target the problems of preterm birth.

In the next paragraph, I will shortly summarise the treatment of preterm born children and possible interventions to protect or restore the affected developmental processes.

1.3 Treatment and restorative interventions in preterm birth

During development, every day is important. This is why it is attempted to delay labour and birth for as long as possible in early labour or high-risk patients (Pediatric nurse 9/13/2021).

Once born, preterm born children undergo many treatments and tests, such as breathing or heart rate monitoring, blood tests, as well as ultrasound scans. Furthermore, there is specialised supportive care for preterm born children, for instance, incubators and feeding tubes or IV fluid supply. Medications include surfactants for respiration, antibiotics in case of infections and other drugs based on the symptoms the children show. Children can leave the hospital once they can breathe and regulate body temperature on their own, are able to feed and have no infections. However, preterm born children can require continuous care and further treatment. (Mayo Clinic 2021b) This further treatment often involves physiotherapy, speech therapy and regular EEG measurements during at least the first 1-2 years, depending on gestational age and condition of the neonate (Pediatric nurse 9/13/2021). This is

why the intensity of neonatal treatment (INTI) is also relevant when investigating the child's development.

A promising intervention is a treatment with erythropoietin (EPO), which has been shown to limit the extent of WMI and neurodevelopmental impairment during childhood, therefore being a neuroprotective measure (Volpe 2019; Rangarajan and Juul 2014). A method for restoring cellular function is treatment with epidermal growth factor (EGF), leading to less cell death and promoting functional recovery (Scafidi et al. 2014). Also, other interventions for changing the phenotype of astrocytes and microglia (Michell-Robinson et al. 2015; Miron et al. 2013; Liddelov and Barres 2017) or treatment with stem cells (Titomanlio et al. 2011) showed favourable effects on pre-oligodendrocyte survival and function.

Another focus in optimal neonatal treatment is on social and environmental factors, such as nutrition and auditory as well as visual experiences to reduce pain and stress (Volpe 2019).

However, these interventions are being researched at the moment, and the effects, as well as side effects, of treatment in neonates have not been studied in detail yet. This means that further research into the causes and consequences of preterm birth is necessary to develop treatments that target the most ideal cells and developmental processes (Volpe 2019).

2 Related Work

In the area of structural impairments after preterm birth, much research has been done by multiple groups. In this chapter, I will summarise the results of previous research and show a graph of known connections between preterm birth, its cellular impacts, and structural changes in the brain.

Many researchers are investigating the effects of preterm birth at various levels: Genes, proteins, as well as structure, cognition and many other measures are studied at different stages of development. Since my thesis is about structure and cognitive abilities, I will summarise the main findings in both fields, mainly in adult subjects and at the time of birth.

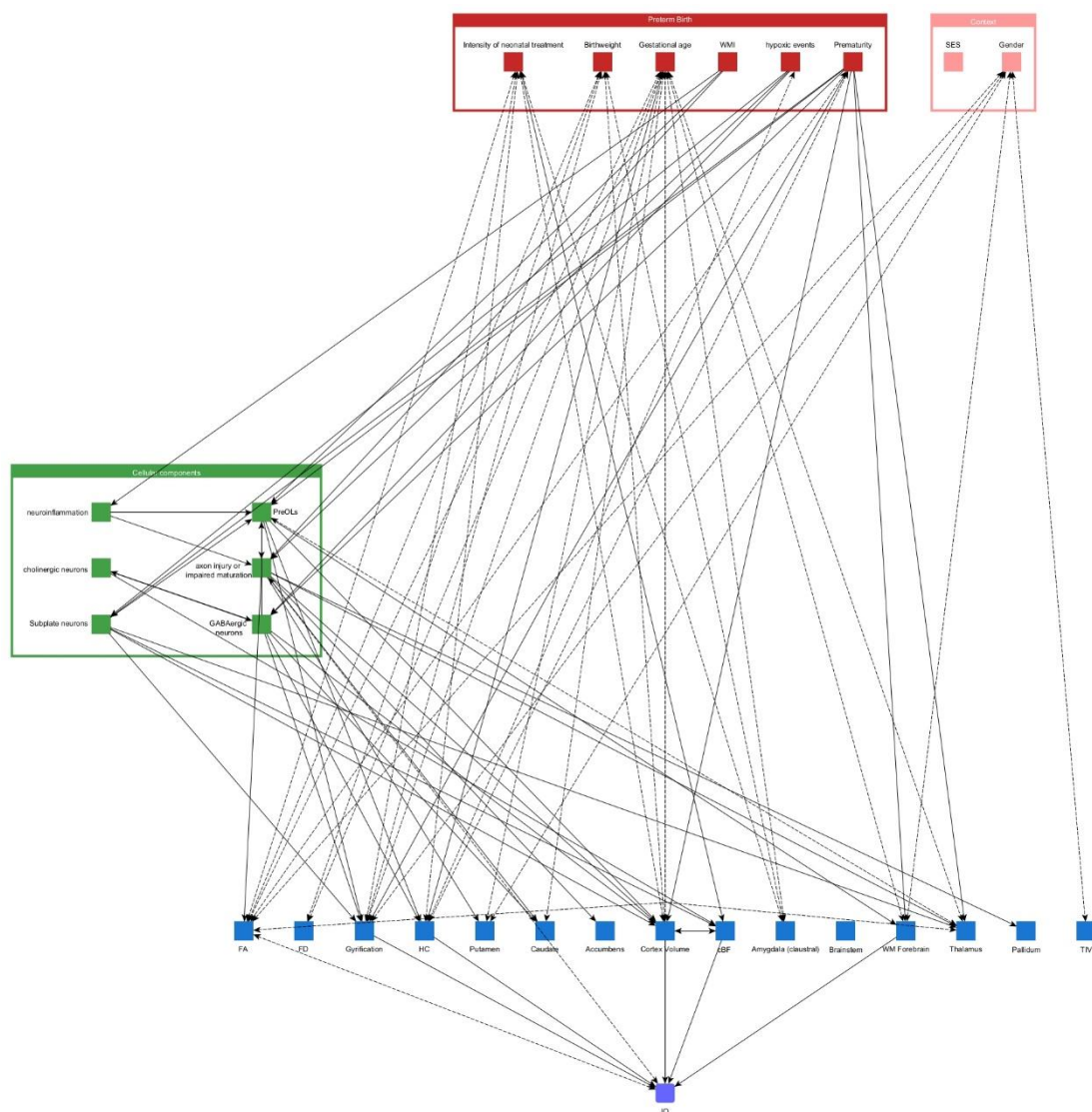


Figure 1 - Graph of relationships in preterm birth, created with yEd (yWorks GmbH 2019)

In Figure 1, an overview of existing research results is shown. On the top, different characteristics of preterm birth are listed in red, for example, the INTI score, gestational age, and birth weight, but also general implications of preterm birth, for instance, white matter injury. Light red marks meta-information, in particular the socio-economic status of the parents and the gender of the child. The microscopic cellular components involved in preterm birth are shown in green, while the macroscopic observations, for example, volumes of structures, gyrification, and diffusion-based measures are

depicted in blue. In this graph, not all investigated macroscopic observations are included, the selection is limited to the variables that show significant differences between preterm- and term-born individuals. Details on the analysis will be explained in chapter 4. Finally, IQ as a proxy for cognitive performance is shown in purple.

First of all, it can be observed that many structural elements (blue) have been linked to preterm birth (red). In turn, many of these structural elements have been linked to IQ (purple). Secondly, much research has been done on finding the cellular mediators of the influence of preterm birth on structure via the cellular level (green). Since the cellular relationships were described in chapter 0, I will focus on the structural findings in this chapter. When referring to the effects of preterm birth, effects of hypoxic-ischemic events or white matter injury in general, low gestational age, low birth weight and intensity of neonatal treatment are summarised for better understanding. Additionally, if not specified otherwise, all observations were made in MRI scans.

Short term. When investigating preterm-born neonates at the time of birth or term-equivalent age, many changes to brain structure were found compared to term-born neonates. Kinney et al. 2012 observed a loss of subplate neurons and GABAergic neurons in a post mortem study of 15 preterm born children and ten control subjects, the loss of GABAergic neurons was also found by Robinson et al. 2006 in 15 preterm born children. Changes in the thalamus were observed by Batalle et al. 2017, including smaller volume and impaired development of connectivity in a group of 65 neonates scanned between GW 24-41. They also observed an impaired development of overall connectivity in the brain in the same cohort. Additionally, Barnett et al. 2018 detected decreased fractional anisotropy with high radial diffusion in this cohort. Boardman et al. 2010 found a smaller volume of both basal ganglia and white matter in a cohort of 80 preterm subjects scanned at term equivalent age and 20 control subjects. At age 7, Zhang et al. 2015 found several changes in cortical development in 24 very preterm born children and 24 control subjects, including altered synaptogenesis, smaller cortical volume, decreased surface area, and aberrant gyrification. Furthermore, in a mouse model, injured white matter axons were observed (Alix et al. 2012), and Buser et al. 2012; Buntinx et al. 2004 discovered white matter injuries. These included especially pre-oligodendrocyte abnormalities along with proinflammatory microglia as well as reactive astrocytes in cell culture and retrospective compared to prospective autopsy cases, respectively.

Long term. When investigating long-term influences of preterm birth on brain development, similar observations to the short-term findings can be made. For instance, reduced grey matter volumes in cortex and subcortex were observed in different cohorts (Amygdala: 101 preterm and 108 controls at age 26 (Schmitz-Koep et al. 2021); hippocampus: 103 preterm and 109 control subjects at age 26 (Hedderich et al. 2020a); cholinergic basal forebrain (cBF): 49 preterm and 59 control subjects at age 18-22 (Grothe et al. 2017); subcortical regions: 99 preterm and 106 control subjects (Meng et al. 2016)). Additionally, Schmitz-Koep et al. 2020 found reduced cortical thickness in 101 preterm and 111 control subjects at age 26, while Hedderich et al. 2020b found reduced cortical complexity, and Hedderich et al. 2019 found aberrant gyrification patterns in the same cohort. Deviations in cortical surface area were detected by Skranes et al. 2013 in a group of 38 preterm and 59 control subjects at age 19. When investigating the white matter, altered volume was described by Nosarti et al. 2014 in 73 preterm and 43 control subjects aged 19-20. Additionally, lower fibre density (group of 73 preterm and 89 controls at age 26, Menegaux et al. 2020) and fractional anisotropy (group of 85 preterm and 69 control at age 25-27 (Meng et al. 2016) as well as 49 preterm and 59 control at age 18-22 (Eikenes et al. 2011)) were discovered. Furthermore, aberrant development of connectivity was detected in cortico-thalamic (Menegaux et al. 2021), resting-state (Bäumli et al. 2015) and intrinsic functional networks (White et al. 2014) in groups of 70 preterm born adults and 67 controls, 96 preterm born

adults and 84 controls at age 25-27 as well as 23 term-born adults at age 27 and 29 very-preterm born adults at age 28, respectively.

Impacts on cognitive performance. Relationships between preterm birth and cognitive performance are, for example, found by Meng et al. 2016; Eikenes et al. 2011, who found that changes in fractional anisotropy lead to changes in cognitive performance. The same relationship was found between changes in gyrification patterns and cognitive performance (Hedderich et al. 2019), as well as changes in the volume of the left dentate gyrus and cognitive performance (Hedderich et al. 2020a). Furthermore, connections between cortical thickness (Schmitz-Koep et al. 2020), cholinergic basal forebrain volume (Grothe et al. 2017), as well as WM forebrain volume (Nosarti et al. 2014) and cognitive performance were observed in MRI scans of preterm born subjects.

Since these factors have all been investigated separately, a correlation analysis will give further insight into the developmental impairments in preterm birth. Additionally, causal analyses were not performed on the topic of preterm birth before, and overall rarely in structural MRI, for example (Pölsterl and Wachinger 2021), so this, too, will yield new understandings.

3 Data

For my thesis, I used data from structural and diffusion-weighted MRI scans, as well as birth-related variables. In the following paragraphs, I will summarise the acquisition and pre-processing of the data used in my thesis.

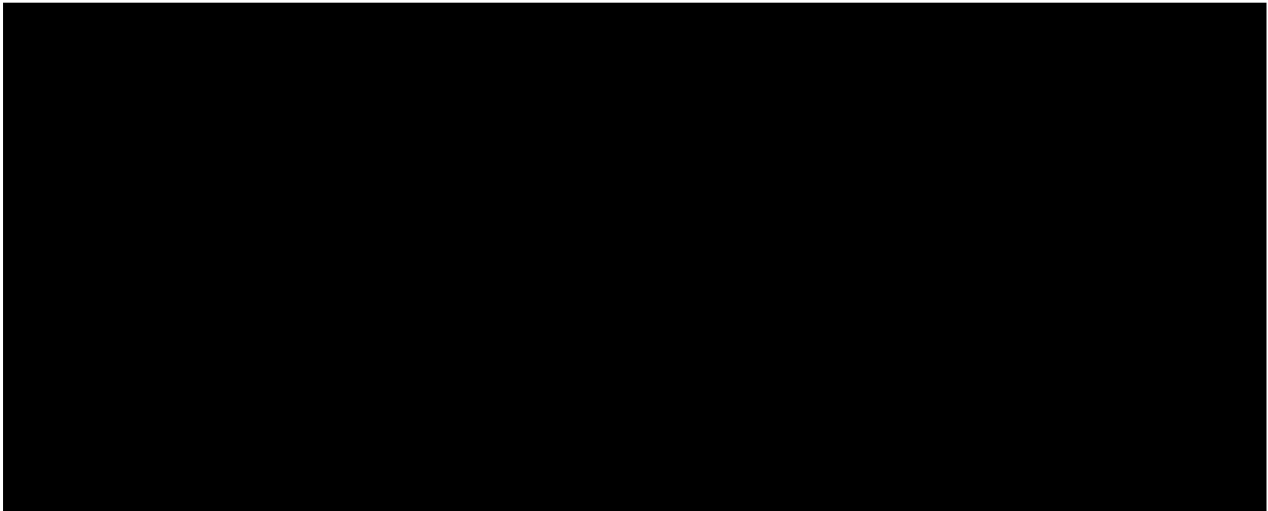


Figure 2 - Demographical, clinical, and cognitive data, taken from (Hedderich et al. 2020b)

3.1 Participant information

The data were acquired in the Bavarian Longitudinal Study (BLS), which observed very preterm-born/very low birth weight (VP/VLBW) children as well as healthy full-term (FT) control subjects during their development from birth until adulthood (Wolke and Meyer 1999; Hedderich et al. 2020b). The BLS measured 682 VP/VLBW subjects born before 32 weeks of gestation and/or birth weight below 1500g. At age 26, 101 VP/VLBW and 111 full-term individuals were scanned in an MRI. The difference between the number of initially recruited individuals and individuals measured at the 26-year follow-up is explained by the exclusion of participants via psychological assessments, MR-related exclusion criteria and lack of motivation of the participants. The control subjects were chosen via stratification variables gender and socio-economic status of the family to be comparable to the study group. (Hedderich et al. 2020b)

MRI scans were performed at the Department of Neuroradiology, Klinikum rechts der Isar, Technische Universität München for 145 subjects and at the Department of Radiology, University Hospital of Bonn for 67 subjects. More details are described in Grothe et al. 2017; Bäuml et al. 2015.

Demographical, clinical, and cognitive data on the cohort can be found in Figure 2. In the VP/VLBW group, cortical and subcortical volumes, as well as gyrification, were measured in 90 patients, cBF volume in 96 participants and diffusion-based measures were measured in 72 patients. In the FT group, cortical and subcortical volumes, as well as gyrification, were measured in 106 patients, cBF volume in 107 participants and diffusion-based measures were measured in 89 patients.

3.2 Data acquisition

Many variables measured in the BLS are used for my thesis. First of all, structural information on the volume on specific cortical and subcortical regions as well as the overall gyrification were recorded in structural MRI. The data were acquired in Philips 3T systems (a Philips Achieva 3T and a Philips Ingenia 3T each in Munich and Bonn) using 8-channel SENSE head-coils. Sequence parameters were identical in all scanners, and dummy-regressors were used to account for scanner-specific differences. The images were acquired by a T1-weighted, 3D-MPRAGE sequence with a reconstructed isotropic voxel size of 1 mm³ (TI=1300ms, TR=7.7ms, flip angle 15°, FOV= 256mm x 256mm) (Hedderich et al. 2020b).

The volumes and gyrification were computed using Freesurfer (Fischl 2012) with the Desikan-Killiany atlas (Desikan et al. 2006).

Secondly, diffusion-based measures, in particular fibre density and fractional anisotropy, were measured using diffusion-weighted imaging. Diffusion-weighted images were acquired using a single-shot spin-echo echo-planar imaging sequence in the same scanners as the structural data, and the results were one non-diffusion weighted image ($b=0$ s/mm²) and 32 diffusion-weighted images ($b=1000$, SENSE factor=2, TE=47ms, TR=20150ms, flip angle=90°, FOV=224mm x 224mm, matrix=112 x 112, 75 transverse slices, slice thickness=2mm, interslice gap=0mm, voxel size=2mm x 2mm x 2mm) (Menegaux et al. 2020). The data were pre-processed and quality controlled using FSL, MRtrix3 and BrainSuite Software (Jenkinson et al. 2012; Tournier et al. 2019; Shattuck and Leahy 2002) in order to extract fibre density and fractional anisotropy maps. Further details can be found in (Menegaux et al. 2020). Regional information was extracted using the John Hopkins University (JHU) -ICBM-DTI-81 WM labels atlas (Mori et al. 2005).

As birth-related variables, gender, gestational age (GA), birth weight (BW), a score for measuring medical complications at birth (intensity of neonatal treatment; INTI), and the socio-economic status of the family at the time of birth (SES) were recorded. GA was estimated from medical reports and assessments, while birth weight was recorded in obstetric records. The INTI score was obtained from a standardised neonatal optimality scoring system (OPTI), and the SES score from an assessment of the profession of the self-identified head of the family and the highest education the parents participated in at the time of birth of the neonate. Further details can be found in (Menegaux et al. 2020; Hedderich et al. 2020b).

One participant was excluded as an outlier for the correlation analysis, and for the causal relationship analysis, only participants with a complete dataset were included, resulting in 60 VP/VLBW subjects.

4 Methods

In this chapter, I will explain in detail my approach to the analyses. These analyses include statistical testing, correlation analysis, similarity analysis, as well as causal inference, all performed in python, version 3.8.10 (van Rossum and Drake 2010).

4.1 Correlation-Analysis

The first step was to analyse the MRI scans and look for significant differences between VP/VLBW and FT adults. Then, in the following steps, I examined the correlation between those differences.

Correlation analysis is being done because brain development and the resulting impairments in preterm birth are such complex processes. Much research has been done to identify separate regions and cell types of interest, but similarities have to be analysed to reduce the intricacy and facilitate further research. This is why correlations and clusters of these correlations will be investigated here.

4.1.1 Categories for different developmental processes of tissue properties

In order to analyse the impact of premature birth on the development of different brain tissues, the data were categorised into five main groups: white matter properties, cortical volume, cortical gyrification, subcortical volumes, and total intracranial volume (TIV). For white matter, the data were further separated into fibre density measurements (FD), fractional anisotropy (FA) and volume of the forebrain, hypointensities as well as cerebellum white matter volume. For the cortical volume and gyrification, all local subregions were included in the computations. As subcortical volumes, amygdala, thalamus, hippocampus, putamen, accumbens area, pallidum, brainstem, cortical cerebellum, and cholinergic basal forebrain (cBF) in both hemispheres, respectively, were selected.

These categories were chosen based on tissue properties and represent separate developmental processes in order to analyse the impact of premature birth on the development of different tissues.

4.1.2 Detection of areas with significant differences and effect sizes

In this paragraph, I will explain how significant differences and effect sizes were computed on the dataset. This was done to identify possible candidates for correlation analyses in order to find meaningful groups of impaired developmental processes.

All available data were combined into a dataset to decide which developmental processes show significant developmental differences in VP/VLBW compared to FT subjects. This dataset included measurements for volumes from the left and right hemisphere, as well as different regional measurements for FA, FD and gyrification all over the brain. First, distributions were checked for similarity with a two-sample Kolmogorov-Smirnov test implemented in SciPy, version 1.6.2 (Virtanen et al. 2020), afterwards, pairwise p-values were calculated using Mann-Whitney-U tests (Mann and Whitney 1947) implemented in Pingouin, version 0.3.11 (Vallat 2018) for these two categories, for each variable, respectively. Next, the p-values were adjusted for multiple testing using Benjamini-Hochberg correction (Benjamini and Hochberg 1995) implemented in statsmodels, version 0.12.2 (Seabold and Perktold 2010). Afterwards, Cohen's delta (Cohen 2013) was computed to measure effect sizes implemented in Pingouin, version 0.3.11 (Vallat 2018).

For further analysis, only variables with significant differences in VP/VLBW compared to FT individuals (adjusted p-value < 0.05) and with an effect size larger than 0.5 were selected.

In the last step, a mean value for all variables of one developmental process was computed for each subject respectively. Consequently, one location-independent representative value was obtained for

each impaired developmental process in each subject. Thus, for example, all measurements belonging to FD all over the brain that showed significant differences between VP/VLBW and FT individuals were combined into one mean value representing the impairments in FD.

4.1.3 Correlation Analysis of developmental disorders

In order to identify groups of similarly impaired developmental processes, a correlation analysis is performed. These correlations will identify developmental processes that develop similarly after impairments by preterm birth.

To compute correlations of the impaired developmental processes, the mean values obtained in the step above were then used as input variables in order to find relationships between impaired developmental processes. The pairwise correlations were analysed using Pearson's r for linear relations, implemented in Pingouin, version 0.3.11 (Vallat 2018). Pearson's r was selected as a correlation measure since, in pairwise plots, relations were found to be mainly linear (see appendix, Figure 38). Finally, correlations were displayed in heatmaps using seaborn, version 0.11.1 (Waskom 2021), and p-values were corrected for multiple testing with Benjamini-Hochberg correction.

4.1.4 Clustering

To determine which developmental processes form correlation clusters, clustering of the Pearson correlation matrix was done using agglomerative hierarchical clustering (Murtagh and Contreras 2012) with Euclidian distance and average linkage implemented in seaborn, version 0.11.1 (Waskom 2021). Agglomerative hierarchical clustering uses a bottom-up approach for linking the most similar groups. Therefore, the resulting dendrogram can be used for assessing similarities between groups. The same clustering algorithm was also used for the variables-participant matrix to check for possible clusters in the participants.

The results obtained from clustering the VP/VLBW and the FT subjects were compared to investigate the differences. Using graph kernels on the created dendrograms, shortest path and graphlet sampling were applied, these kernels are implemented in GraKel, version 0.1.8 (Siglidis et al. 2020). Shortest path kernels firstly separate graphs in their shortest paths and consequently analyse pairs of these shortest paths based on length and labels of endpoints. Similarly, graphlet sampling kernels create subgraphs of the input graphs and compare matching graphlets from both input graphs (Siglidis et al. 2020). Additionally, the edit distance between the graphs (Zhang and Shasha 1989) was computed using zss, version 1.2.0 (Tim Henderson 2021), representing the number of deletions, insertions and replacements being performed in order to transform one graph into the other.

To assess reproducibility, the results of correlation-clustering were compared to the results of sparse principal component analysis (sparse PCA) on normalized data (Cai et al. 2013), which is a tool for dimensionality reduction with an additional constraint on the sparseness of the resulting eigenvectors, therefore making interpretations easier. The implementation of sparse PCA in scikit-learn, version 0.24.2 (Pedregosa et al. 2011) was used.

4.2 Causal Relationship Analysis

In this paragraph, the approach to identifying causal effects between structural measures and cognitive performance is explained.

Causal inference is the process of estimating causal effects. A variable has a causal effect on an outcome if different values of the variable lead to different outcomes. In reality, however, every subject is only exposed to one value of the variable, and therefore, only one value can be observed for the outcome. So, because the rest of the observations are missing, no causal effect can be

measured. However, in a study cohort, the variable and the outcome are potentially different for each participant, so only an average causal effect in this population can be estimated. (Hernán and Robins 2020)

Causation measures the outcome in the same population under different treatments, while association measures the outcome in two subsets of a population that each undergoes a different treatment value (Hernán and Robins 2020). However, to estimate these causal effects, every variable-outcome combination would have to be observed in every subject respectively. In our case, we are analysing an observational study, which also allows inferring causal effects, as long as the identifiability condition holds. This condition is true if the posterior distribution can be estimated from the observed joint distribution, which applies in our case.

The causal question asked in this approach is "What is the average causal effect of changing structural measures (volumes, gyrification, FA, FD) on cognitive performance (IQ) in VP/VLBW adults?"

In order to analyse which variables have an influence on cognitive performance, causal analysis was performed. The approach was based on research for causation in Alzheimer’s disease (Pölsterl and Wachinger 2021), who combined a deconfounding approach (Wang and Blei 2019) with Bayesian estimation to account for unobserved confounders.

For finding causal relationships, the first step is to develop a causal graph that represents all available data and the respective connections based on expert knowledge and literature review. In our case, the graph (compare Figure 3) shows the influence of the impaired developmental processes on cognitive performance – the confounders in this scenario-, and on the other hand, the influences of birth-related and social variables on these developmental processes and cognitive performance. Since it is not known what influence the birth-related and social variables have on the relationship between developmental processes and cognitive performance, and furthermore, whether any other confounders are not observed, the deconfounding approach is applied as a next step before analysing the causal relationships in the last step. (Pölsterl and Wachinger 2021)

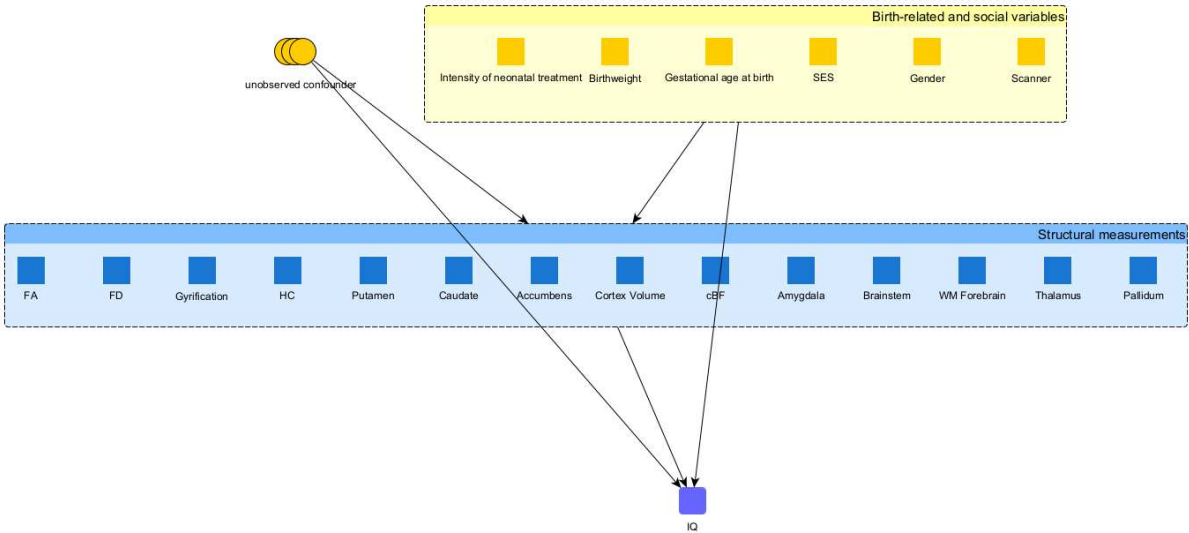


Figure 3 - causal graph, created with yEd (yWorks GmbH 2019)

The algorithm applied was firstly PPCA (Tipping and Bishop 1999) for deconfounding and secondly Bayesian linear regression (Box and Tiao 1992), both using probability distributions to estimate the parameters.

Data preparation included splitting the participants into a train- and a test-set and normalizing both based on the train-set. Afterwards, the variables in train-and test-set together were separated into assigned causes, in this case being MRI-derived measures on the one hand and meta-information on the other hand, including socio-economic status, gender, birth weight, gestational age, the intensity of neonatal treatment, and the scanner. These data were then passed to the deconfounding step.

Step 1 - Deconfounding. In most cases, measured data are confounded both by observed and unobserved confounders. Confounders are defined as hidden variables that have influence both on the assigned causes and on the potential outcome, implying a correlation of causes and outcome as well as biased estimates of causal inference. If these observed and unobserved multiple-cause confounders are simultaneous of interest, a deconfounder can be used. With the deconfounding algorithm proposed by Wang and Blei 2019, both observed and unobserved confounders can be included in the analysis while making weaker assumptions than other causal inference models. To do this, unsupervised machine learning is combined with predictive model checking. Therefore, a latent variable model representing the relations between variables is fitted and used to predict the latent variable for each subject, providing a substitute for unobserved confounders (Wang and Blei 2019). This substitute makes the assigned causes independent and therefore suited for causal inference. The latent variable model used in my thesis is probabilistic principal component analysis (PPCA) (Tipping and Bishop 1999). The PPCA model is fit on a part of the data, while some datapoints are held back as a test-set that is being used later. The assumptions for using the deconfounder are that the latent-variable model represents the assigned causes well and that there are no unobserved single-cause confounders. This stands in contrast to the common assumption of causal inference models having no unobserved confounders at all. This is done because this assumption of no unobserved confounders rarely holds in practice (Pölsterl and Wachinger 2021). For assessing the results of PPCA, Bayesian p-values with expected negative log-likelihood as a test statistic are computed by comparing simulated datapoints drawn from the posterior predictive distribution with the previously held out data (Pölsterl and Wachinger 2021). Only sufficient representations of the causes (Bayesian p-value > 0.1) are accepted. As a last step, posterior mean estimates and the reconstruction of the causes are computed. The identifiability of causal effects of neuroanatomical measures and a substitute confounder has been proven in (Pölsterl and Wachinger 2021) with Pearl's do-calculus (Pearl 2000), which I will not go into detail on as it is outside the scope of this thesis.

Step 2 – Bayesian linear regression. After deconfounding the data, causal analysis can be performed to predict IQ from MRI-derived measures and the substitute confounder. The input data were the reconstructed causes instead of the original MRI derived measures to account for the unobserved confounder. To do this, the train-test split is recreated, and Bayesian linear regression (Box and Tiao 1992) with a t-distribution for the likelihood of the targets is used to model the effects of impaired developmental processes on cognitive performance. This approach was chosen based on the observed normal distribution for IQ as a target (see appendix, Figure 39). Priors were normal distributions with a mean of 0 and a standard deviation of 10, and the degrees of freedom were modelled using an exponential distribution. Bayesian linear regression yields results for the model parameters as posterior probability distributions via samples drawn using no-U-turn Monte-Carlo sampling in `pystan`, version 2.19.1.1 (Riddell et al. 2021). Also, predictions for a test set have been made. The highest density intervals representing the posterior distribution for the resulting draws are plotted both for the deconfounded and the non-deconfounded data to assess significance. The reliability of the results is controlled in posterior predictive checks.

To summarize, causal analysis is done by removing the impact of possible observed and unobserved confounders on the assigned causes, the MRI-derived measures in this analysis. These adjusted assigned causes are then used to analyse their significance in the relationship to the effect, in this

case, IQ. These significances can then be interpreted as information on causal relationships between causes and effect.

5 Results

In the first part of my master's thesis, I followed the research question, "Are there correlations between differences in developmental processes?". In order to answer the question, it was separated into subquestions that I will be elaborating on in the following chapter. These subquestions are:

1. What are the developmental processes relevant for the information that can be obtained from MRI scans?
2. Which of these developmental processes show significant differences between VP/VLBW and FT individuals?
3. Which of these significant differences in developmental processes are correlated?

The second part of my thesis answers the question, "What are the causal relationships between the MRI-derived measures that show significant differences between VP/VLBW and FT individuals and IQ?".

In this chapter, I will present the results of these questions.

5.1 Subquestion 1: What are the different developmental processes?

As explained in chapter 4.1.1, the available variables were sub-categorised into five main groups: white matter properties, cortical volume, cortical gyrification, subcortical volumes, and total intracranial volume (TIV). These categories were selected based on the microstructure of the tissues and represent different developmental processes.

5.2 Subquestion 2: Which developmental processes have significant differences between VP/VLBW and FT individuals?

Significant differences were computed between VP/VLBW and FT individuals using Mann-Whitney-U Tests (Mann and Whitney 1947) and correction for multiple testing with Benjamini-Hochberg correction (Benjamini and Hochberg 1995) as well as effect sizes (Cohen 2013) (see chapter 4.1.2). Significant differences (corrected p-value < 0.05 and Cohen's d > 0.5) have been found in cortical volume, cortical gyrification, FA, FD, white matter forebrain volume and subcortical volumes. The significantly different subcortical volumes were amygdala, thalamus, hippocampus, nucleus accumbens, putamen, pallidum, brainstem, cholinergic basal forebrain, and caudate volumes. Detailed results can be found as a table in the appendix (Chapter 9.1), and visualisations will be shown in the next paragraphs.

5.2.1 Visualisations of significantly different cortical and subcortical volumes

Figure 4 - Figure 9 depict the cortical regions that show significantly different volumes in VP/VLBW and FT born adults. These regions are in the right hemisphere, the banks of the superior temporal sulcus, inferior parietal lobe, isthmus of the cingulate gyrus, lateral orbitofrontal cortex, middle temporal gyrus, orbital part of the inferior frontal gyrus, posterior cingulate cortex, rostral anterior cingulate cortex, superior parietal lobe, and supramarginal gyrus. In the left hemisphere, inferior parietal lobe, isthmus of the cingulate gyrus, lateral orbitofrontal cortex, middle temporal gyrus, orbital part of the inferior frontal gyrus, precentral gyrus, and superior parietal lobe volumes are significantly different.

For the subcortical volumes in Figure 10 and Figure 11, nucleus accumbens in both hemispheres, the amygdala in both hemispheres, brainstem, caudate in both hemispheres, cholinergic basal forebrain, hippocampus in both hemispheres, pallidum in both hemispheres, putamen in the right hemisphere, and thalamus volumes in both hemispheres are significantly different between VP/VLBW and FT adults.

In these figures, colour is only used for the distinction of different regions and does not represent an order of any kind.

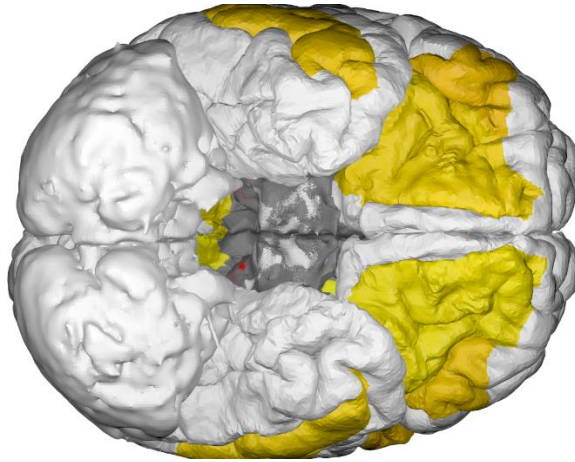


Figure 4 - Significant developmental differences in cortical volume (bottom view); highlighted are the lateral orbitofrontal cortices, cingulate cortices, orbital part of the inferior frontal gyri, and middle temporal gyri. Created with BrainPainter (Marinescu et al. 2019).

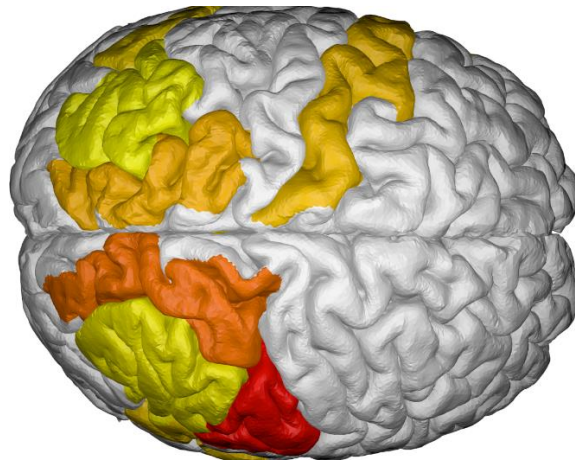


Figure 5 - Significant developmental differences in cortical volume (top view); highlighted are the parietal cortices (superior and inferior), supramarginal gyrus, and the precentral gyrus. Created with BrainPainter (Marinescu et al. 2019).

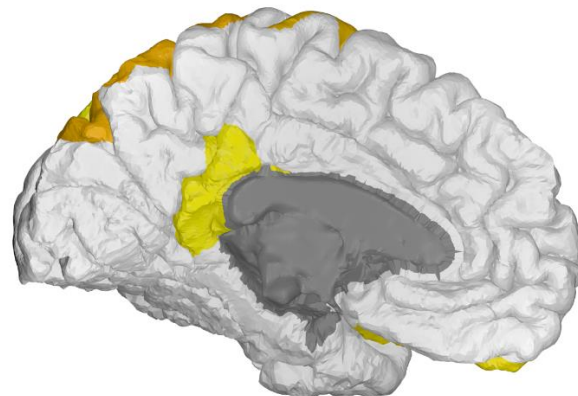


Figure 6 - Significant developmental differences in cortical volume (inner left hemisphere); highlighted are the isthmus of the cingulate cortex, as well as the superior parietal and lateral orbitofrontal cortex. Created with BrainPainter (Marinescu et al. 2019).

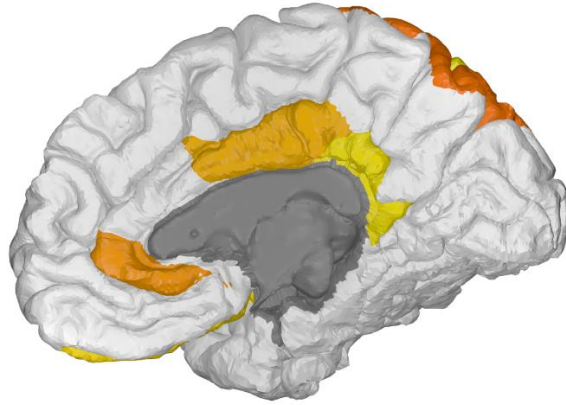


Figure 7- Significant developmental differences in cortical volume (inner right hemisphere); highlighted are the cingulate cortex (isthmus, posterior, and rostral anterior part), as well as superior parietal and lateral orbitofrontal cortex. Created with BrainPainter (Marinescu et al. 2019).

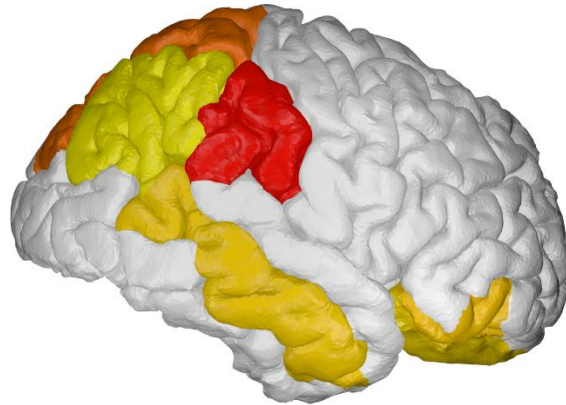


Figure 8- Significant developmental differences in cortical volume (outer right hemisphere); highlighted are the lateral orbitofrontal cortex, orbital part of the inferior frontal gyrus, middle temporal gyrus, parietal cortices (superior and inferior), banks of the superior temporal sulcus, and supramarginal gyrus. Created with BrainPainter (Marinescu et al. 2019).

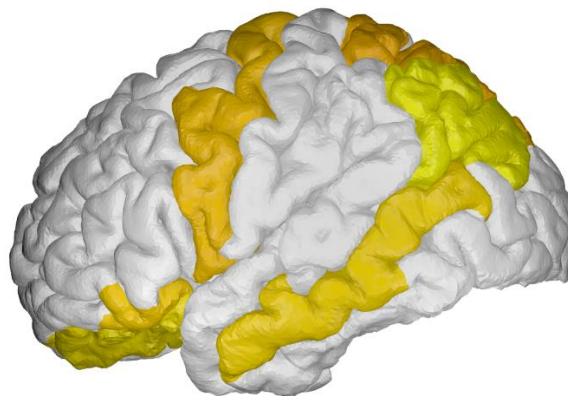


Figure 9- Significant developmental differences in cortical volume (outer left hemisphere); highlighted are the lateral orbitofrontal cortex, orbital part of the inferior frontal gyrus, middle temporal gyrus, parietal cortices (superior and inferior), and the precentral gyrus. Created with BrainPainter (Marinescu et al. 2019).

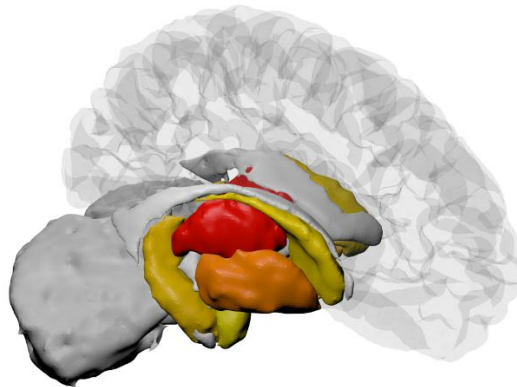


Figure 10 - Significant developmental differences in subcortical volume (right hemisphere); highlighted are the nucleus accumbens, amygdala, caudate, hippocampus, pallidum, putamen, and thalamus. Created with BrainPainter (Marinescu et al. 2019).

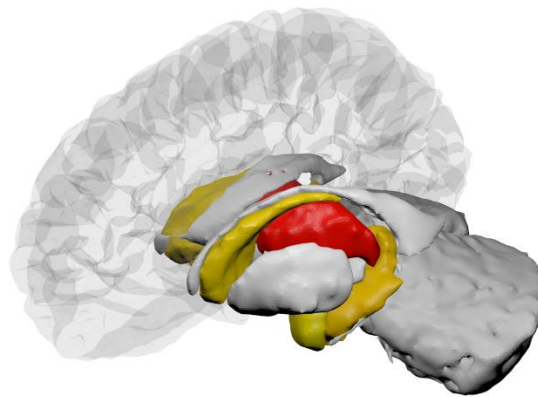


Figure 11 - Significant developmental differences in subcortical volume (left hemisphere); highlighted are the nucleus accumbens, amygdala, caudate, hippocampus, pallidum, and thalamus. Created with BrainPainter (Marinescu et al. 2019).

5.2.2 Visualisations of areas with significantly different cortical gyrification

In Figure 12 - Figure 17, significant differences in cortical gyrification between VP/VLBW and FT born adults are visualised. These regions are in the right hemisphere lateral occipital gyrus, middle temporal gyrus, pars opercularis, pars orbitalis and pars triangularis of the inferior frontal gyrus, postcentral gyrus, superior parietal lobe, superior temporal gyrus, transverse temporal gyrus, as well as insular lobe. In the left hemisphere, cuneus, middle temporal gyrus, pars opercularis of the inferior frontal gyrus, pericalcarine cortex, precuneus, superior parietal lobe, superior temporal gyrus, transverse temporal gyrus, and insular lobe show significant differences in gyrification.

As before, in these figures, colour is only used for the distinction of different regions and does not represent an order of any kind.

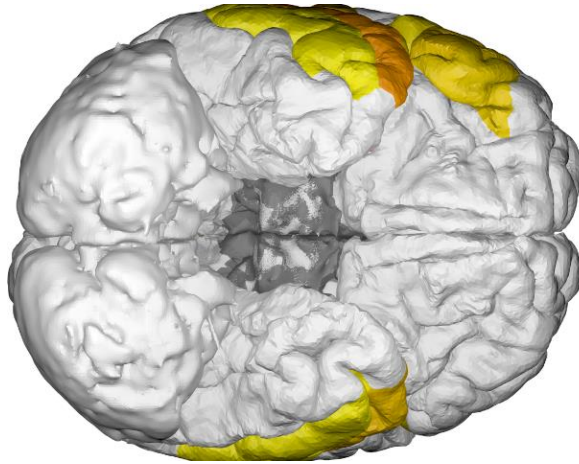


Figure 12 Significant developmental differences in gyrification (bottom view); highlighted are middle temporal gyri, middle temporal gyri, and superior temporal gyri. Created with BrainPainter (Marinescu et al. 2019).

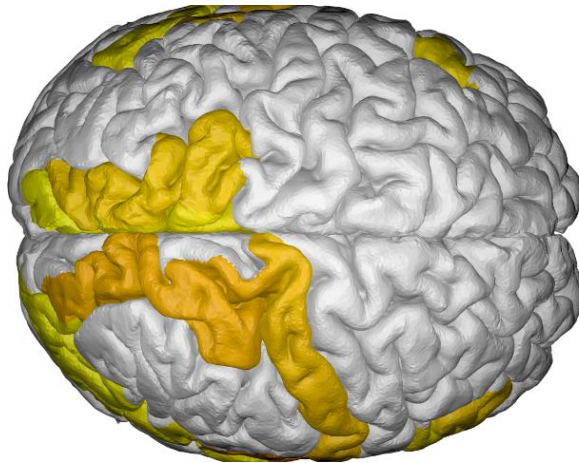


Figure 13 Significant developmental differences in gyrification (top view); highlighted are pars opercularis (both hemispheres) and pars triangularis of the inferior frontal gyrus, postcentral gyrus, and superior parietal lobes. Created with BrainPainter (Marinescu et al. 2019).

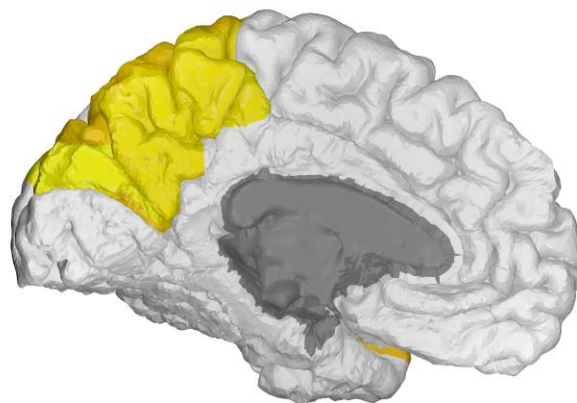


Figure 14 Significant developmental differences in gyrification (inner left hemisphere); highlighted are superior parietal lobe, cuneus, precuneus, and pericalcarine cortex. Created with BrainPainter (Marinescu et al. 2019).

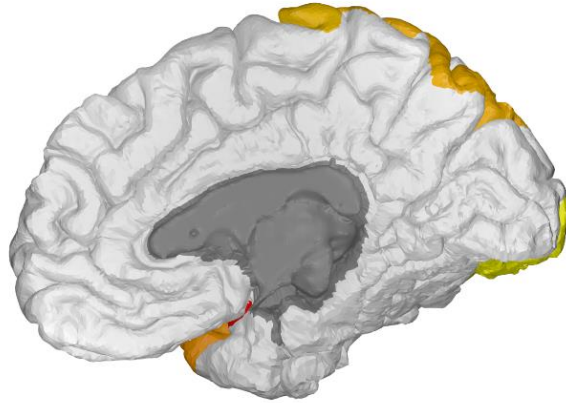


Figure 15 - Significant developmental differences in gyrification (inner right hemisphere); highlighted are lateral occipital gyrus and superior parietal lobe. Created with BrainPainter (Marinescu et al. 2019).

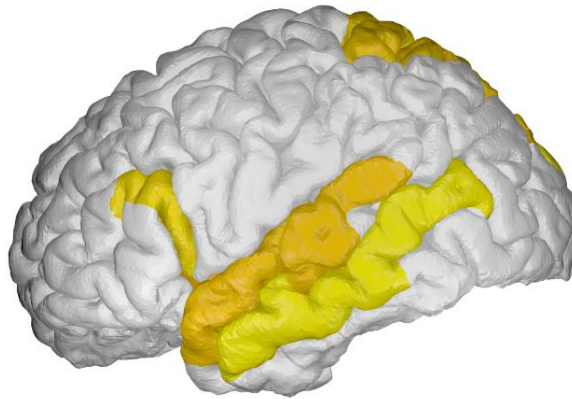


Figure 16 Significant developmental differences in gyrification (outer left hemisphere); highlighted are middle temporal gyrus, pars opercularis of the inferior frontal gyrus, superior parietal lobe, superior temporal gyrus, transverse temporal gyrus, and insular lobe. Created with BrainPainter (Marinescu et al. 2019).

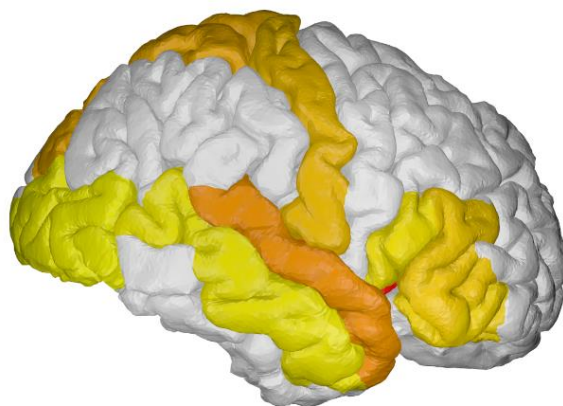


Figure 17 Significant developmental differences in gyrification (outer right hemisphere); highlighted are lateral occipital gyrus, middle temporal gyrus, pars opercularis, pars orbitalis and pars triangularis of the inferior frontal gyrus, postcentral gyrus, superior parietal lobe, superior temporal gyrus, transverse temporal gyrus, and insular lobe. Created with BrainPainter (Marinescu et al. 2019).

5.2.3 White matter properties with significant differences

The white matter properties that showed significant differences between VP/VLBW and FT born adults are white matter forebrain volume in both hemispheres, as well as specific areas in FA and FD.

When looking at FA differences, the body of corpus callosum, column and body of fornix, superior cerebellar peduncle in both hemispheres, right cerebral peduncle, external capsule in both hemispheres, cingulate gyrus in both hemispheres, left fornical crus/stria terminalis, uncinata fasciculus in both hemispheres, as well as left tapetum showed significant differences.

The significant differences in FD were observed in genu, body, and splenium of the corpus callosum, column and body of fornix, superior cerebellar peduncle in both hemispheres, right cerebral peduncle, left external capsule, right cingulate gyrus, fornical crus/stria terminalis in both hemispheres, right uncinata fasciculus as well as left tapetum.

To summarize the findings, significant differences between VP/VLBW and FT born adults were found in various grey and white matter structures. These structures will be the starting point for the further analyses looking into similarities in the significant impairments of developmental processes in the VP/VLBW group.

5.3 Subquestion 3: Which significant differences in developmental processes are correlated?

For identifying similarities in impaired development after VP/VLBW birth, correlations and clusters of these correlations were computed. These clusters are then used to identify groups of developmental processes that exhibit similar differences in VP/VLBW compared to FT born adults.

After computing the significant differences, for each significantly impaired developmental process, a mean value per subject was computed (see chapter 4.1.2). This was done to focus on the processes and create a representative value independent of regional indices. In this chapter, I will describe the findings.

5.3.1 Correlation Matrices

In Figure 18 and Figure 19, the correlations between significantly impaired developmental processes in VP/VLBW and FT born adults, respectively, are depicted.

In VP/VLBW born adults, it can be seen that especially high correlations are between FD and FA ($r=0.91$), while further high correlation can be seen in the combinations thalamus - pallidum volume, caudate - accumbens volume, accumbens - cBF volume, cBF – pallidum volume, as well as the hippocampus - amygdala volume ($r \geq 0.75$). On the other hand, especially low correlations can be observed between gyrification and caudate, brainstem, putamen, as well as FA ($r \leq 0.25$).

Conversely, the highest correlations in term-born adults are in the combinations of white matter forebrain volume – thalamus volume and hippocampus – amygdala volume ($r \geq 0.75$). Furthermore, the lowest correlations were observed in multiple combinations of FD/FA – cortical/subcortical volumes/gyrification ($r \leq 0.25$).

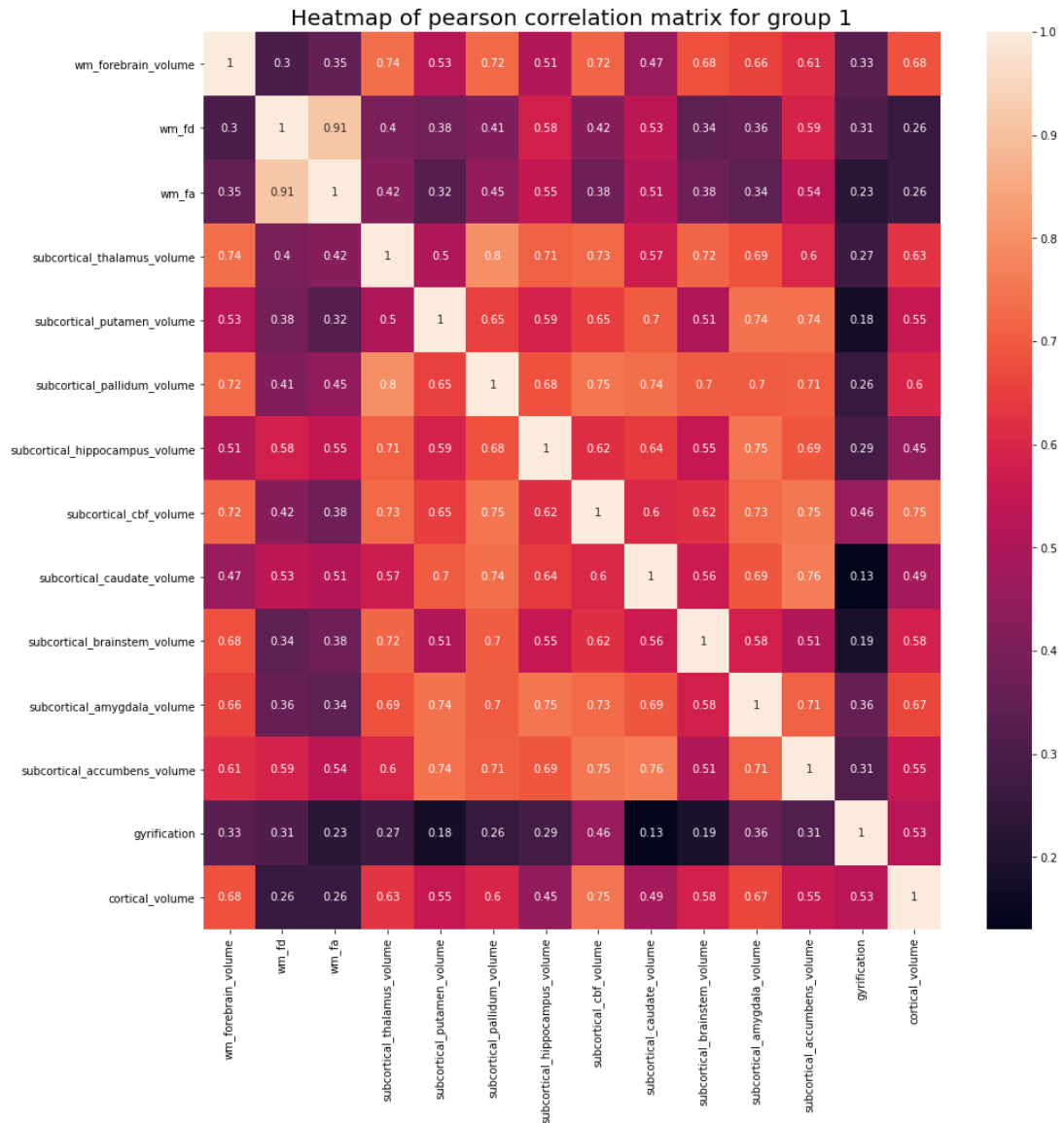


Figure 18 - Heatmap of Pearson correlation of significantly different developmental processes in the VP/VLBW group

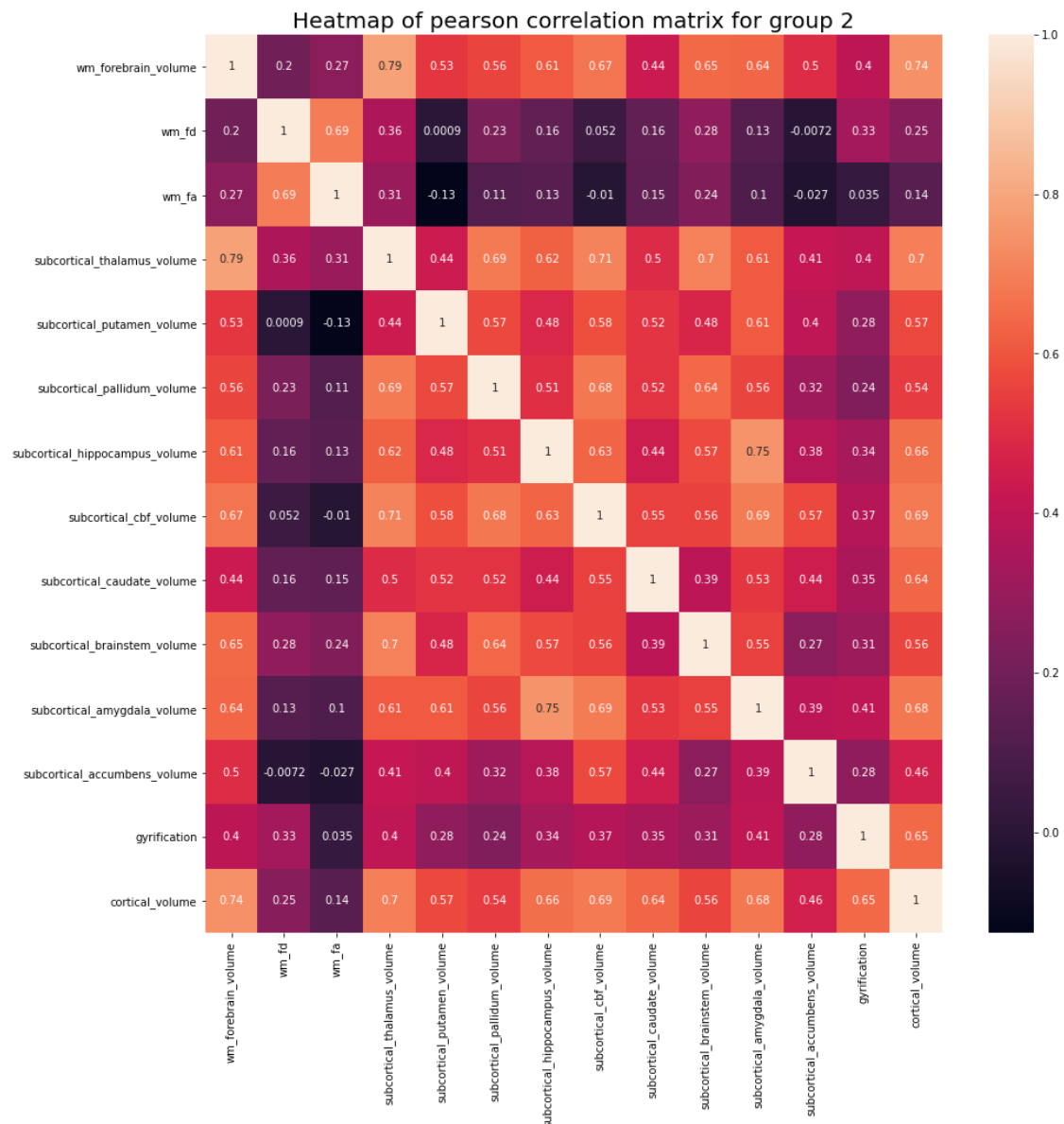


Figure 19 - Heatmap of Pearson correlation of significantly different developmental processes in the FT group

5.3.2 Clusters in Correlation Matrices

As can already be seen when looking at the results of the correlation analyses, clusters of correlations can be observed. Using agglomerative hierarchical clustering (Murtagh and Contreras 2012) (see chapter 4.1.4), dendrograms representing these clusters were computed both for VP/VLBW and FT born adults based on similarity of the correlations. Based on these similarities, clusters and subclusters can be separated.

In VP/VLBW born adults (Figure 20), the first cluster consists of cortical gyrfication, therefore representing the least similarity to other measures. The rest of the variables are further subdivided into a cluster containing FA as well as FD, and in the same way, another cluster of hippocampus, putamen, caudate and nucleus accumbens volumes is split off.

In FT born adults (Figure 21), on the other hand, the first split separates FA and FD from the rest of the measures. Then, in another division, gyrfication is separated from the rest of the variables, in which could be divided into accumbens volume and further into more minor splits. However, no further unambiguous separation can be observed.

The dendrograms obtained with hierarchical clustering can be compared using multiple measures (see chapter 4.1.4). Based on graph kernels, the result of the shortest path comparison is 0.973, while the result of graphlet sampling is 0.946, the edit distance is 23. These results show that the clusterings of VP/VLBW and FT born adults are not the same but similar.

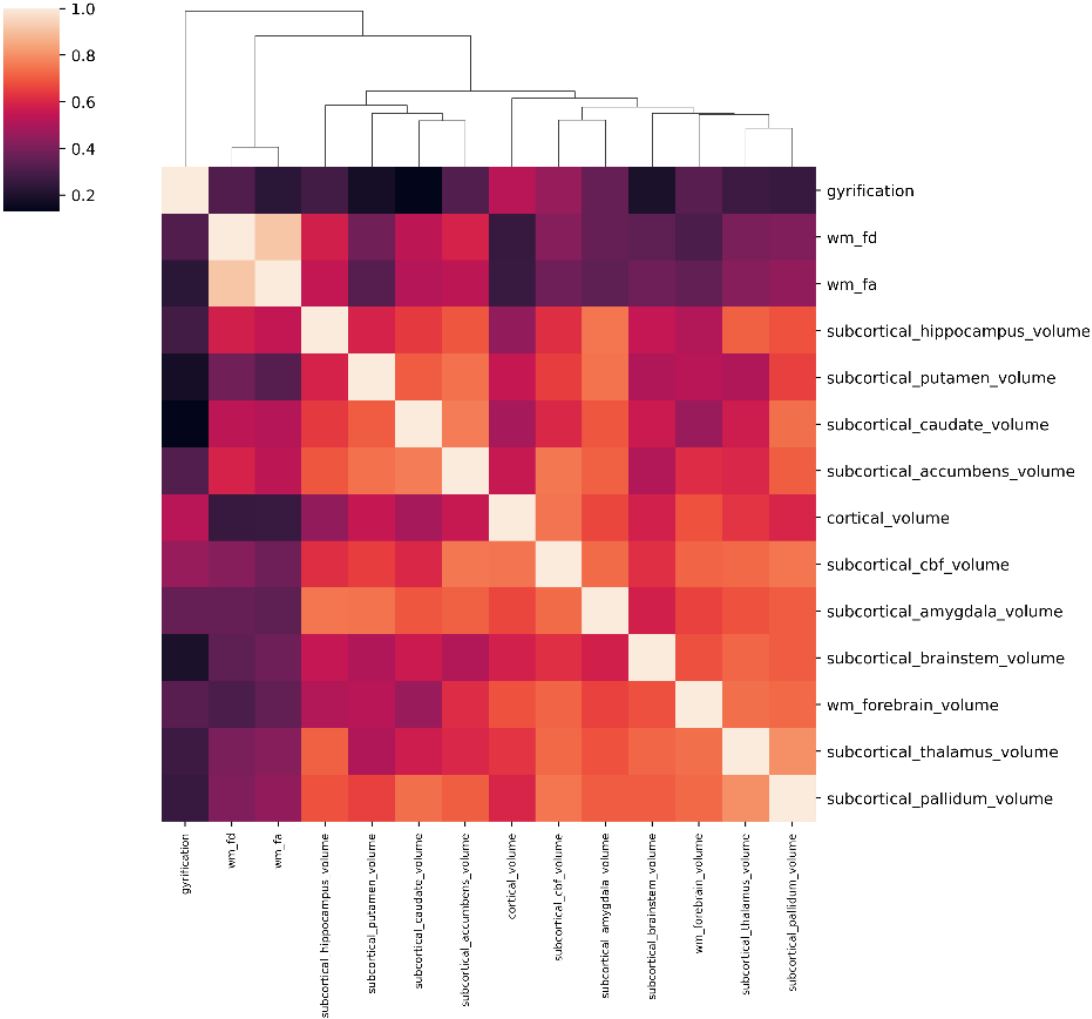


Figure 20 - Clustergrid for Pearson correlation based on euclidean distance metric, VP/VLBW group

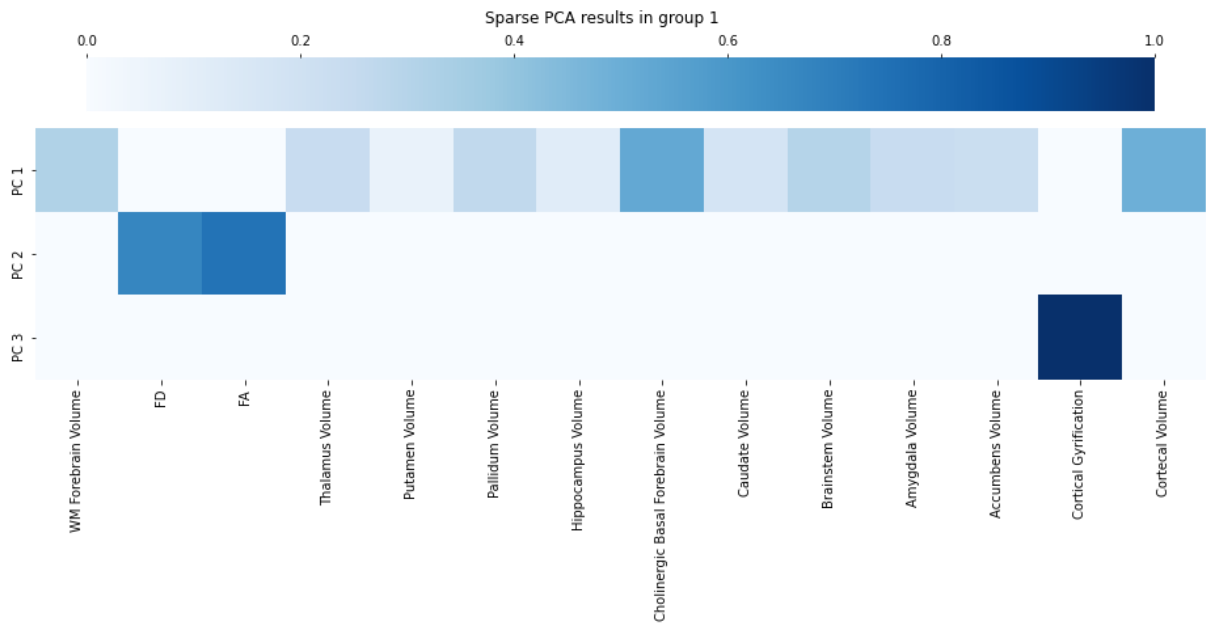


Figure 22 - Sparse PCA results for three principal components in the VP/VLBW group

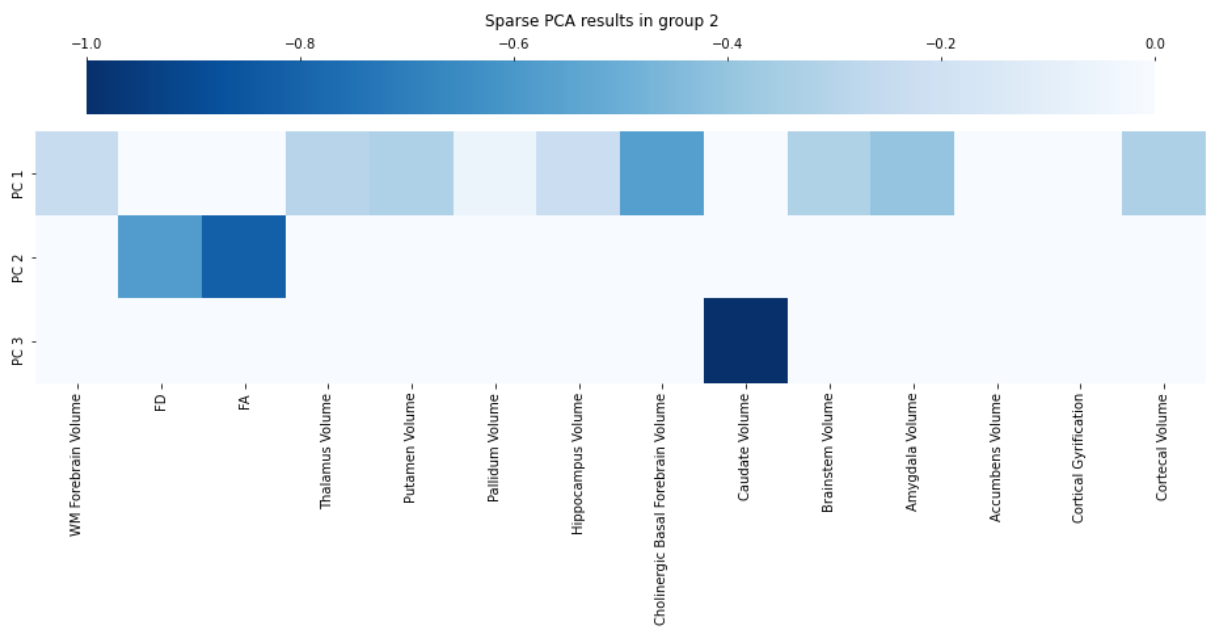


Figure 23 - Sparse PCA results for three principal components in the FT group

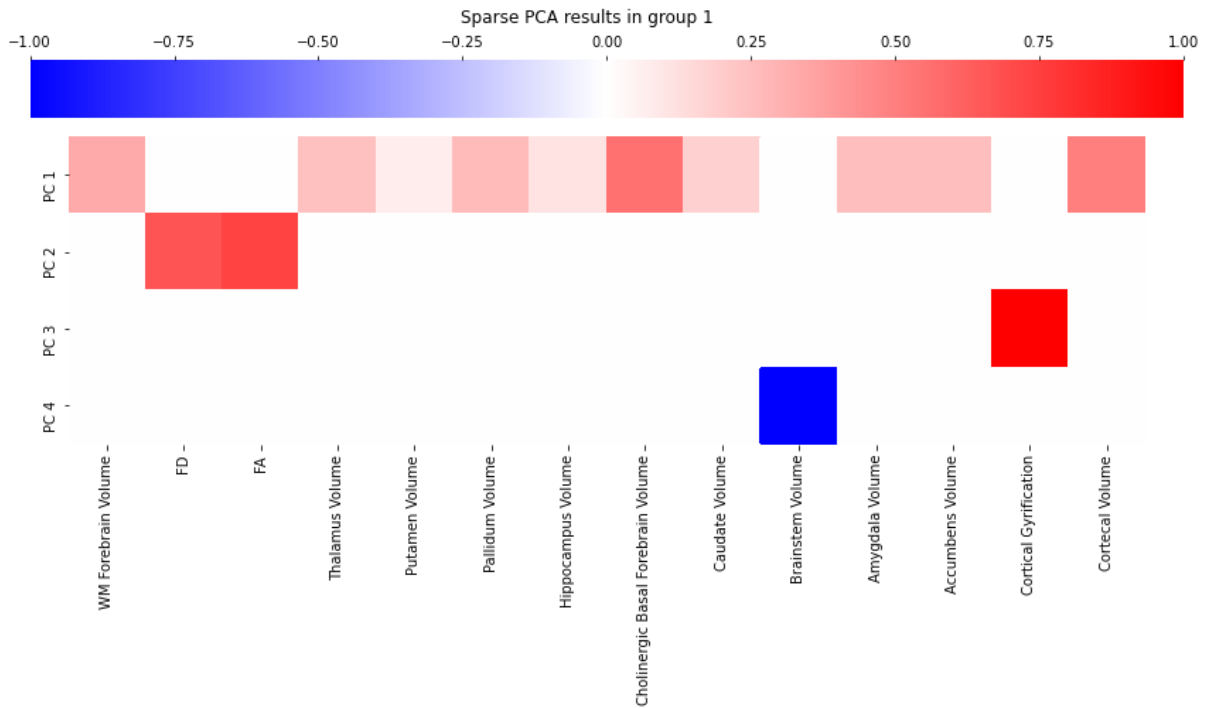


Figure 24 - Sparse PCA results for four principal components in the VP/VLBW group

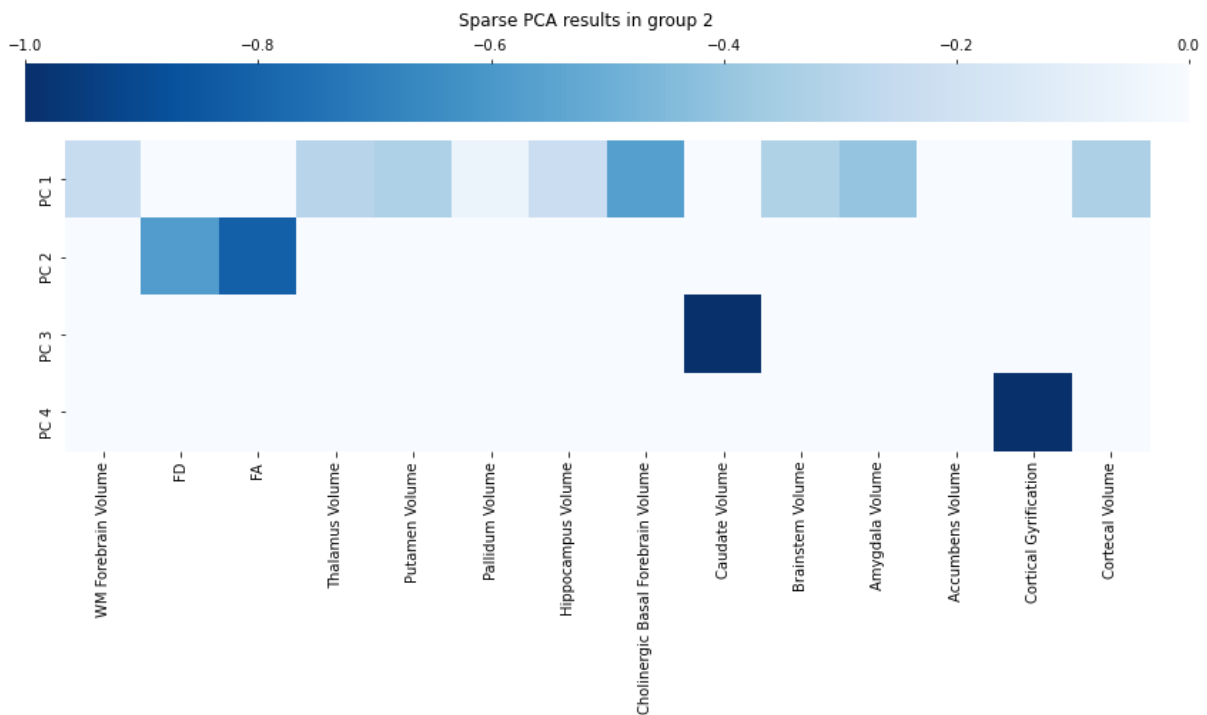


Figure 25 - Sparse PCA results for four principal components in the FT group

5.3.4 Clusters in Participant Matrix

The same hierarchical agglomerative clustering algorithm for the correlations can also be applied to the participant-variable matrix, using the original data instead of correlations. As shown in Figure 26, in VP/VLBW born adults, three major groups can be identified. One group contains one single participant with high values for most of the variables. Another group can be identified as 12 subjects that mainly have low values for the variables, and the third group is made up of the rest of the

participants, containing mixed values. These types of groups cannot be seen in the term-born adults (Figure 27), however, a group of two participants with low values for most variables can be identified.

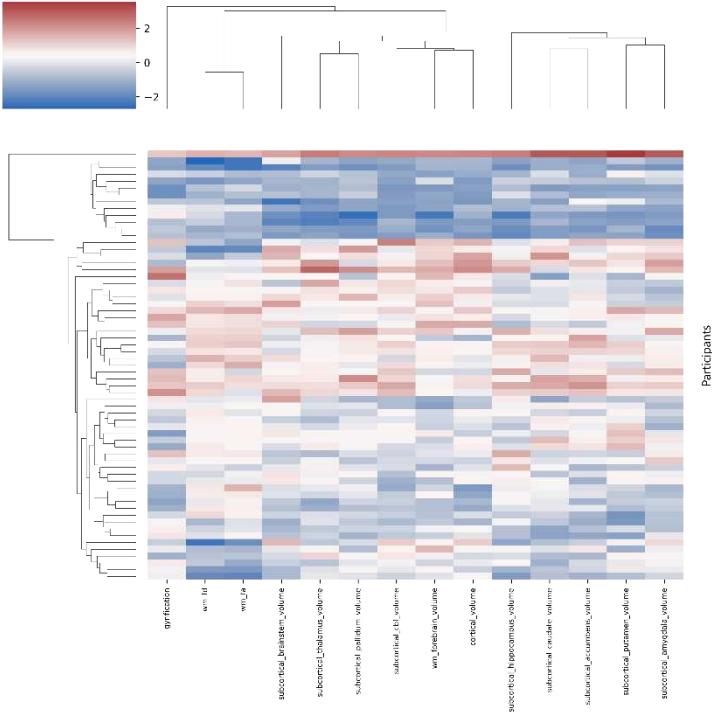


Figure 26 - Clustering on participants-variable matrix, preterm-born adults

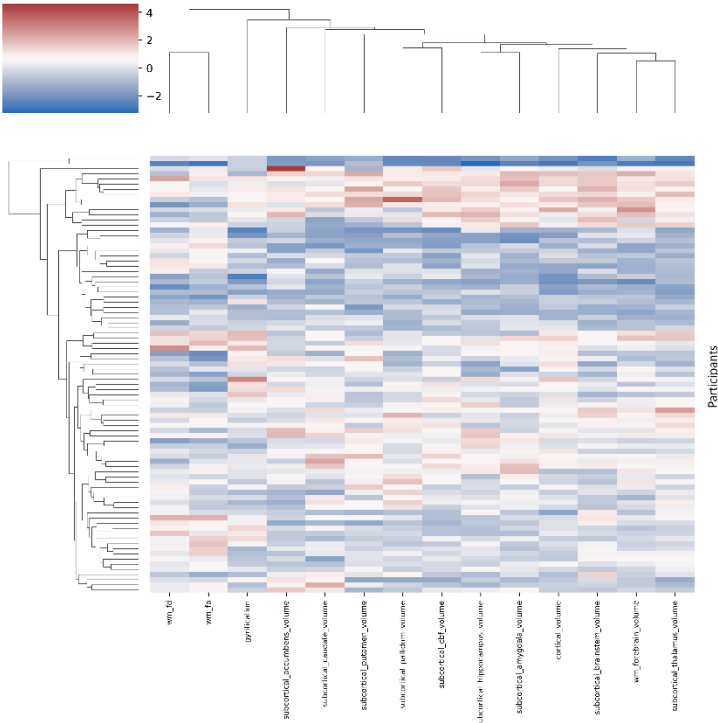


Figure 27 - Clustering on participants-variable matrix, term-born adults

Summarising the results for the first research question, "Are there correlations between differences in developmental processes?", it can be found that there are significant differences in developmental processes in VP/VLBW compared to FT born adults. Furthermore, these significant differences are

correlated and can be grouped based on similarities. These groupings differ in the VP/VLBW and FT groups. A detailed discussion of the results can be found in chapter 6.1.

5.4 Subquestion 4: "What are the causal relationships between the MRI-derived measures that show significant differences between VP/VLBW and FT born individuals and IQ?"

To answer the question "What are the causal relationships between the MRI-derived measures that show significant differences between VP/VLBW and FT born individuals and IQ?", causal analysis was performed based on Bayesian linear regression and deconfounding (see chapter 4.2). The analyses were performed both on deconfounded and original data to be comparable. For deconfounding with PPCA based on one unobserved confounder, the Bayesian p-value was 0.807.

I will present the results both for analysis with and without deconfounding in this chapter. These results can also be seen in Figure 28 and Figure 29, with bars representing the highest density intervals. In blue, results of the deconfounded data are displayed, while orange represents the original data without deconfounding. Negative results imply that if the value of the variable is higher, IQ is lower, and positive results can be interpreted as the higher the value, the higher IQ. A result is significant if it does not cross the line at 0.

Deconfounded data. We found that thalamus volume, cholinergic basal forebrain volume, caudate volume, brainstem volume, and amygdala volume are causally relevant with a positive relationship for analysing the cognitive performance based on IQ when looking at the 75% highest density interval (HDI) in the deconfounded model (see Figure 28, blue). Negative causal relationships were found in putamen volume and cortical gyrification. Furthermore, in the 97.5% HDI, we found that thalamus volume is positively causally relevant for analysing the cognitive performance based on IQ (see Figure 29, blue).

These results can also be observed when plotting the effect sizes (Figure 30 - Figure 36). The positive effects are in the effect of thalamus volume on IQ (Figure 36), where a volume increase of 1000 mm³ leads to an IQ that is approximately 15 points higher, as well as cBF volume (Figure 34, an increase of 200 mm³ leads to an about 20 points higher IQ), caudate volume (Figure 33, an increase of 1000 mm³ leads to an increase of about 7 IQ points), brainstem volume (Figure 32, an increase of 1000 mm³ leads to an about 3 points higher IQ), and amygdala volume (Figure 31, an increase of 1000 mm³ leads to an about 3 points higher IQ). On the other hand, negative effects can be seen in the effect of putamen volume on IQ (Figure 35), where an increase in volume of 1000 mm³ has an approximately 8 points lower IQ as a consequence, as well as cortical gyrification (Figure 30), where an increase of the gyrification index by 0.5 leads to a decreased IQ of about 11 points. The effect sizes for the non-causally relevant results can be found in the appendix (Figure 40-Figure 47).

Original data without deconfounding. When looking at the 75% HDI intervals in the model without deconfounding, we found that thalamus volume, cholinergic basal forebrain volume, brainstem volume, and amygdala volume are significant with a positive relationship when analysing the cognitive performance (see Figure 28, yellow). Additionally, white matter forebrain volume, putamen volume, and cortical gyrification were negatively significant. On the other hand, in the 97.5% HDI, we found that the cholinergic basal forebrain is positively significant for analysing the cognitive performance based on IQ (see Figure 29, yellow).

These results show that the data are confounded by the observed confounders gestational age, gender, INTI, scanner, and one or possibly more unobserved confounders. This is demonstrated by the differences between deconfounded and non-deconfounded results in Figure 28 and Figure 29. It can be observed that the influence of white matter forebrain volume, caudate volume, and thalamus

volume was confounded by the confounders since the decision about whether there is a causally relevant relationship in the model has been changed by deconfounding. In addition, apart from the shifts in causal relevance, especially thalamus volume is confounded in the original data, based on the significant shift in value this variable's distribution shows.

However, since in the posterior predictive check (Figure 37), the posterior is not perfectly aligned with the observed data, implying that the model does not perfectly fit the data, the interpretation has to be done carefully. Therefore, more work on this topic is needed to make more meaningful observations.

To summarize the results for the question "What are the causal relationships between the MRI-derived measures and IQ?" it can be said that there is at least one unobserved confounder that influences the measures. After deconfounding, multiple developmental processes were found to be causally linked to IQ in the VP/VLBW group. An in-depth discussion can be found in chapter 6.2.

Estimated parameters for causal influence of structure on IQ, 75 percent HDI, t-distribution

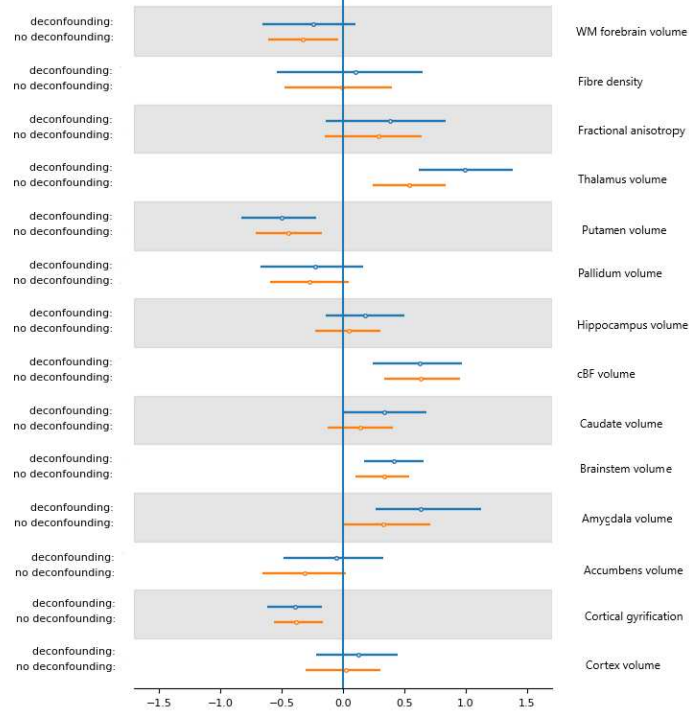


Figure 28- Results of causal analysis for deconfounded and non-deconfounded data, shown are 75% HDI

Estimated parameters for causal influence of structure on IQ, 97.5 percent HDI, t-distribution

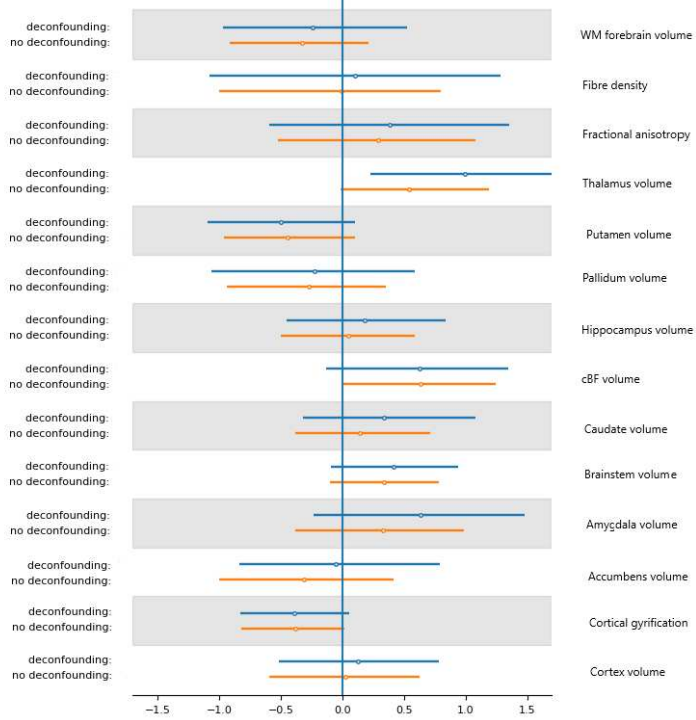


Figure 29 - Results of causal analysis for deconfounded and non-deconfounded data, shown are 97.5% HDI

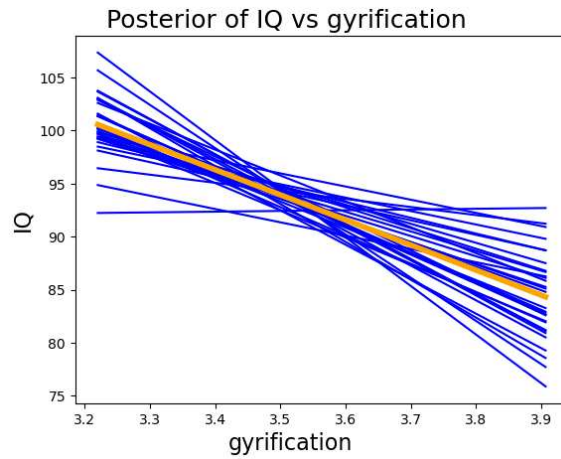


Figure 30 - Effect size of cortical gyrification on IQ, blue depicts predictions by drawing from the posterior distribution, orange depicts mean of predictions

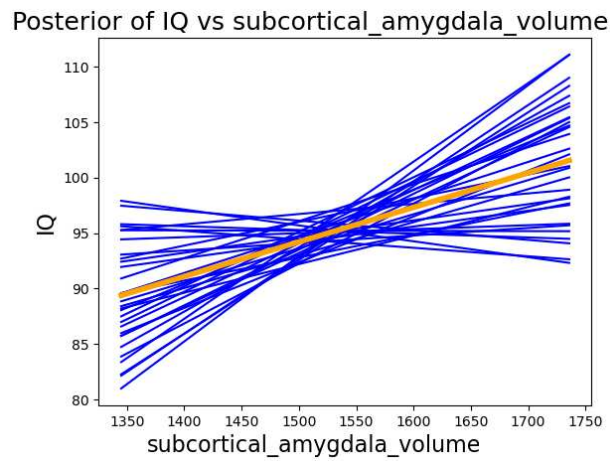


Figure 31 - Effect size of amygdala volume on IQ, blue depicts predictions by drawing from the posterior distribution, orange depicts mean of predictions

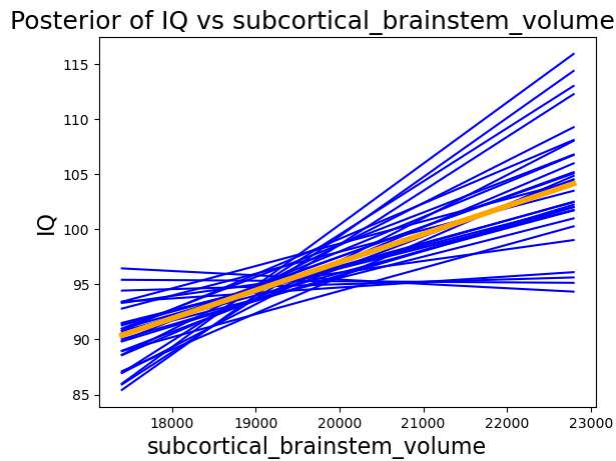


Figure 32 - Effect size of brainstem volume on IQ, blue depicts predictions by drawing from the posterior distribution, orange depicts mean of predictions

Posterior of IQ vs subcortical_caudate_volume

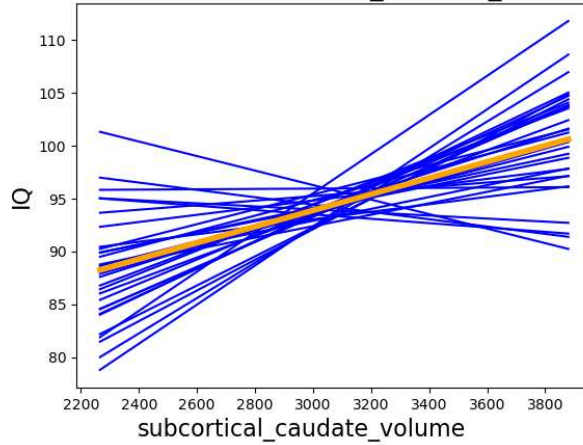


Figure 33 - Effect size of caudate volume on IQ, blue depicts predictions by drawing from the posterior distribution, orange depicts mean of predictions

Posterior of IQ vs subcortical_cbf_volume

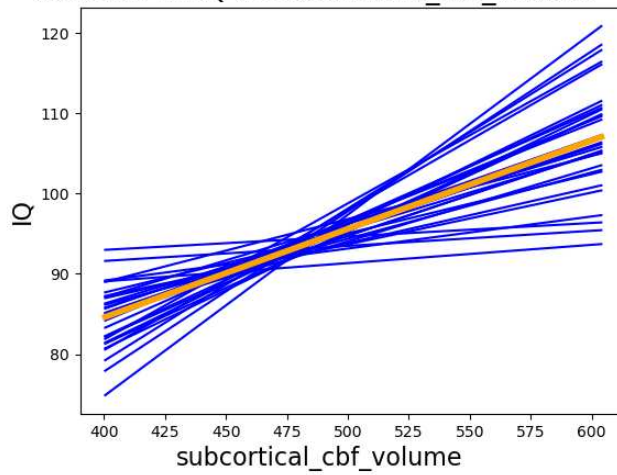


Figure 34 - Effect size of cBF volume on IQ, blue depicts predictions by drawing from the posterior distribution, orange depicts mean of predictions

Posterior of IQ vs subcortical_putamen_volume

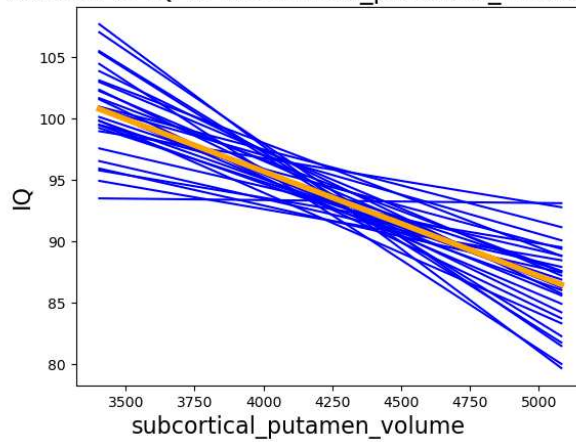


Figure 35 - Effect size of putamen volume on IQ, blue depicts predictions by drawing from the posterior distribution, orange depicts mean of predictions

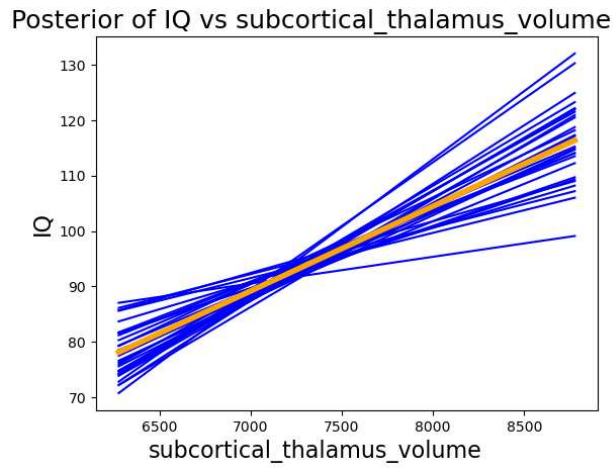


Figure 36 - Effect size of thalamus volume on IQ, blue depicts predictions by drawing from the posterior distribution, orange depicts mean of predictions

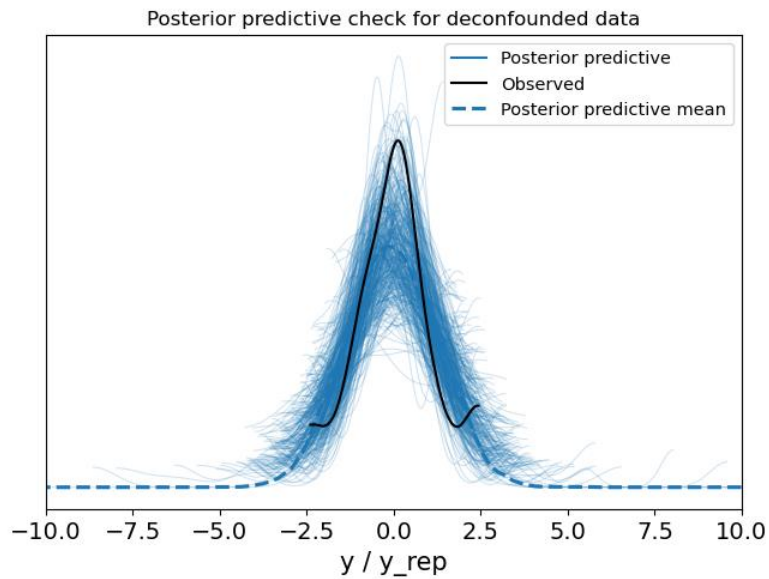


Figure 37 - Posterior predictive check for the linear regression model

6 Discussion

In this chapter, I will discuss and interpret the results presented in chapter 5. Therefore, I will answer the research questions and analyse whether the results agree with previous research.

6.1 "Are there correlations between differences in developmental processes?"

In the first part of my thesis, I researched the question, "Are there correlations between differences in developmental processes?". I found that indeed there are developmental processes that are significantly different in VP/VLBW birth compared to FT birth and, furthermore, that these developmental processes are correlated and can be categorised into groups based on similarity.

The first cluster, containing cortical gyrification only, could be explained by the distinct process of gyrification that is not directly related to volumes or connectivity, but rather a combination of those as well as possible other mechanisms, for instance, genetics. In contrast, the fact that gyrification is more similar to other measures in term-born adults shows that gyrification could be a key target of impairment in VP/VLBW birth and is supported by differences in gyrification patterns found by Hedderich et al. 2019.

The second cluster containing FD and FA implies that FD and FA develop more similar to each other than to other measures. It could be explained by the fact that both measure connectivity based on diffusion-weighted MRI. Since preterm birth is known to affect axonal development both via direct influence as well as via impaired myelination, and on the other hand, affect connectivity in several cortical and subcortical networks, FA and FD being not that similar to other measures could be explained. Additionally, differences in FA and FD in VP/VLBW born adults were also reported by Menegaux et al. 2020. The observation that FA and FD together form a more distinct cluster in FT adults compared to VP/VLBW born adults could be caused by the fact that gyrification is a much more distinctly impaired developmental process in VP/VLBW born adults than in FT born adults.

In the same way, the third similarity cluster containing hippocampus, putamen, caudate nucleus, and nucleus accumbens could be explained by the fact that putamen, caudate nucleus as well as nucleus accumbens together are all part of the basal ganglia and therefore developmentally closely related. Additionally, the hippocampus is connected to the basal ganglia via the ventral striatum consisting of the nucleus accumbens (David Smith and Paul Bolam 1990). Differences in basal ganglia as well as in hippocampus development in VP/VLBW subjects were not surprising since they already were reported by Volpe 2019 and Hedderich et al. 2020a. This is also possibly why, in term-born adults, this effect is not as outstanding. Research suggests that both basal ganglia and hippocampus are involved in memory and learning, although in different ways (Shohamy et al. 2009), which could also hint towards related development.

Significant differences in the measures in the last cluster, cortical volume, cBF, brainstem, white matter forebrain, thalamus, globus pallidus and amygdala volumes also come to no surprise since Nosarti et al. 2014 reported differences in the thalamus and brainstem volumes, Volpe 2019 wrote about differences in thalamic, cortical and white matter volumes, while Schmitz-Koep et al. 2021 reported decreased amygdala volumes. Additionally, Loh et al. 2017 observed lower pallidum volumes in VP/VLBW born children at the age of 7 years, which could be caused by the fact that the pallidum mainly contains GABAergic neurons that are highly vulnerable to hypoxic events. The grouping could fit since especially cortex and thalamus are highly connected, and white matter represents these connections among others (Menegaux et al. 2021). The same is true for the brainstem, which is connected to the thalamus (Krout et al. 2002), the amygdala (connections to cortex and brainstem (Liddell et al. 2005)), cBF (having cholinergic connections to the cortex) (Semba 1991) and the globus pallidus, which connects to the cortex via the thalamus (Kemp and Powell 1971).

Interestingly, not all parts of the basal ganglia are grouped into one similarity cluster, which could be caused by the globus pallidus being an output nucleus, while caudate, putamen and nucleus accumbens are input nuclei (Groenewegen 2003).

The fact that sparse PCA can support these clusters underlines the expressiveness of these results.

In the FT group, three main clusters were identified that differed from the VP/VLBW groups in the order and arrangement of included developmental processes. This could be caused by processes that are altered explicitly in VP/VLBW birth, while others are less severely impaired and therefore separated into different groups. In the FT group, however, this separation would not occur, so the groups would not be as distinctive.

Overall, the highest correlations in VP/VLBW born adults were observed between FD and FA, which could be explained by both measuring WM fibre tracts (see above). Further high correlations between subcortical volumes could also be expected since they are highly connected, and all suffer from neuronal and axonal damage during preterm birth. On the other hand, the lowest correlations between gyrification and FA or subcortical volumes could be explained by the fact that gyrification, FA and subcortical volumes represent different developmental processes and develop following different time courses.

Additionally, the differences in correlations in the VP/VLBW compared to the FT group could be caused by the same reasons possible for explaining the differences in the clustering. Here, again, impairments in VP/VLBW birth could lead to differences in development that are shared between developmental processes and, therefore, more correlated in the FT group than the VP/VLBW group. Additionally, the same could be true for the differences in the lowest correlation. Here, different impairments could apply to different developmental processes and therefore make them less correlated.

Other interesting observations were the subgroups in VP/VLBW born subjects, which could be due to impacts of gender or birth-related variables but could also have other reasons. Therefore, further research is needed to possibly identify different types of effects of preterm birth.

To conclude, the correlations we found in our analyses resulted in plausible insights into correlations in developmental processes of VP/VLBW born adults. These analyses have not been performed before and pave the way for further research that focuses on the groups we identified.

6.2 "What are the causal relationships between the MRI-derived measures and IQ?"

In the second part of my thesis, I investigated possible causal effects between the MRI-derived measures that showed significant differences in VP/VLBW compared to FT born adults and cognitive performance using deconfounding and causal inference.

We found that deconfounding with one additional unobserved confounder had an effect on the results, implying that apart from birth weight, gestational age at birth, gender, socio-economic status and scanner used, at least one other variable influences either MRI-derived measures, cognitive performance, or both. This could be explained by preterm birth being a highly complex topic involving multiple causes and effects. However, further research is needed to identify these additional possible confounders and their impact on the topic of preterm birth.

The causal relationships that were identified were the connection between thalamus volume and IQ, which was significant in a 97.5% HDI. Since the thalamus is mainly involved in attention, information processing and memory, a strong causal relationship is not surprising (Amin and Ontaneda 2020). Further causally relevant relationships were found between putamen volume, cholinergic basal

forebrain volume, caudate volume, brainstem volume, amygdala volume, as well as cortical gyrification and IQ, however with less certainty. These results are explainable by the fact that the basal ganglia, including putamen and nucleus caudate, are involved in learning (Shohamy et al. 2009), while the amygdala is involved in emotional responses, long-term memory, working memory as well as attention (Schaefer and Gray 2007). Furthermore, brainstem nuclei have been found to be involved in cognition (Köhler et al. 2016). A contribution of gyrification to the impact of premature birth on cognitive performance was also reported by Hedderich et al. 2019, who found that aberrant gyrification, especially in lateral temporal association cortices being associated with IQ impairments in VP/VLBW born adults via a mediation analysis. The same effect was also found in a mediation analysis by Grothe et al. 2017 for the cholinergic basal forebrain in VP/VLBW born adults, being explained by the role of cBF in cognitive functions. Therefore, this causal analysis provides further indication for gyrification as well as cBF and the other identified causes being an essential target for risk prediction and drug targeting. An essential result of the causal analyses are the effect sizes of these causally relevant relationships, which validate the findings and are useful for risk prediction.

Interestingly, the hippocampus, being hypothesised to be one of the main components involved in memory formation and retrieval (Andersen et al. 2006), does not seem to have a causal relationship with cognitive performance. This could be the case because other measures already explain the effect of hippocampus volume on differences in cognition, however, further research is needed.

This causal analysis yields important results since, for the first time, not only associations but also causations can be observed in the context of preterm birth. In contrast to the causal findings, when not using the deconfounding approach, in the 75% HDI, white matter forebrain volume is significant, while caudate volume is not significant for analysing cognitive performance. In the 97.5% HDI, thalamus volume is insignificant, and cholinergic basal forebrain volume is significant. The rest of the causally relevant variables are also significant in the analysis without deconfounding. These differences could be due to these measures representing developmental differences that are, in fact, caused by one of the confounders. Still, since they are not considered in this non-causal analysis, the effect seems to come from the measure itself. On the other hand, insignificant variables in the original data can become causally relevant because the confounders mask their effect. These influences of the confounders are then reversed by applying deconfounding.

To conclude, we performed the first causal analysis on the impacts of impaired developmental processes on cognitive performance in VP/VLBW born adults. While these results have to be interpreted carefully, our results are plausible since we considered unobserved confounders. Furthermore, with this approach, we identified causal relationships that had not been identified before.

6.3 Strengths and limitations

In my thesis, some limitations are present. Firstly, the dataset is biased towards participants with less severe complications at birth since more complications make exclusion from MRI more likely. This makes the estimated effects conservative estimates of the actual effects in the complete cohort. Additionally, the socio-economic status can change over the course of 26 years, and since it was only assessed at birth and not during the course of development, it may bias the data. On the other hand, the large sample size of 101 VP/VLBW born children and 111 FT controls makes the results robust and generalisable. Furthermore, the effect of age on brain development is excluded in these analyses since all participants were roughly examined at the same age (26 years). The recording of the MRI scans in four different scanners could contribute bias to the data, even though this effect was accounted for during pre-processing. Also, the present dataset only represents the development at one point in time, so for further research, longitudinal studies are needed to investigate the findings during brain

development from birth until adulthood. More information on the limitations of the dataset can be found in (Hedderich et al. 2019). Another important point is that the causal analysis must be interpreted carefully due to an imperfect fit in the posterior predictive check, and further analyses are needed to find a better-suited model. This model could incorporate non-parametric Gaussian processes and therefore avoid our assumption of linearity. However, causal analysis is a strong tool to investigate relationships since directed relationships can be identified compared to associations in other analyses. Additionally, the deconfounding approach with the inclusion of unobserved confounders allows finding causal relationships without strong assumptions, some of these relationships would not have been found without accounting for unobserved confounding.

7 Conclusion

In conclusion, we developed a comprehensive graph of related literature, created models, interpreted the results, found an answer to both research questions and paved the way for further research on the topic of preterm birth by finding interesting new questions.

The answer to the first research question, "Are there correlations between differences in developmental processes?" is yes, there are correlations between impaired developmental processes. These impairments can be found in many but not all investigated developmental processes, and, furthermore, the observed correlations can be grouped into 4 clusters based on similarity.

The answer to the second question, "What are the causal relationships between the MRI-derived measures that show significant differences between VP/VLBW and FT born individuals and IQ?", shows for the first time that thalamus volume, putamen volume, cholinergic basal forebrain volume, caudate volume, brainstem volume, amygdala volume and cortical gyrification are causally relevant for IQ with high certainty.

The implications for preterm-born children are that the correlations and causal relations we found could inform new targets for drugs and inform further research. Also, especially the causal relationships could inspire new ways of risk assessment for cognitive function in preterm-born neonates. In this context, the open questions are how accounting for regional indices influences these results and what findings can be made. Another question is how the clusters we found could be explained and whether they can be replicated on other datasets, and lastly, how our findings in adults can be transferred to preterm-born children.

Additional further research should consider whether VP/VLBW born adults or children can be grouped into subgroups and how the causal analysis could be improved to make more reliable observations.

To summarise, this thesis applied new approaches in the area of research on preterm birth and contributed previously unknown insights as well as further research questions.

8 Publication bibliography

- Alix, James J. P.; Zammit, Christian; Riddle, Art; Meshul, Charles K.; Back, Stephen A.; Valentino, Mario; Fern, Robert (2012): Central axons preparing to myelinate are highly sensitive corrected to ischemic injury. In *Annals of neurology* 72 (6), pp. 936–951. DOI: 10.1002/ana.23690.
- Amin, Moein; Ontaneda, Daniel (2020): Thalamic Injury and Cognition in Multiple Sclerosis. In *Front. Neurol.* 11, p. 623914. DOI: 10.3389/fneur.2020.623914.
- Andersen, Per; Morris, Richard; Amaral, David; Bliss, Tim; O'Keefe, John (2006): *The Hippocampus Book*: Oxford University Press.
- Anderson, Peter J.; Treyvaud, Karli; Neil, Jeffrey J.; Cheong, Jeanie L. Y.; Hunt, Rodney W.; Thompson, Deanne K. et al. (2017): Associations of Newborn Brain Magnetic Resonance Imaging with Long-Term Neurodevelopmental Impairments in Very Preterm Children. In *The Journal of Pediatrics* 187, 58-65.e1. DOI: 10.1016/j.jpeds.2017.04.059.
- Back, Stephen A. (2017): White matter injury in the preterm infant: pathology and mechanisms. In *Acta Neuropathol* 134 (3), pp. 331–349. DOI: 10.1007/s00401-017-1718-6.
- Back, Stephen A.; Luo, Ning Ling; Borenstein, Natalia S.; Volpe, Joseph J.; Kinney, Hannah C. (2002): Arrested oligodendrocyte lineage progression during human cerebral white matter development: dissociation between the timing of progenitor differentiation and myelinogenesis. In *J Neuropathol Exp Neurol* 61 (2), pp. 197–211. DOI: 10.1093/jnen/61.2.197.
- Back, Stephen A.; Luo, Ning Ling; Borenstein, Natalya S.; Levine, Joel M.; Volpe, Joseph J.; Kinney, Hannah C. (2001): Late Oligodendrocyte Progenitors Coincide with the Developmental Window of Vulnerability for Human Perinatal White Matter Injury. In *J. Neurosci.* 21 (4), pp. 1302–1312. DOI: 10.1523/JNEUROSCI.21-04-01302.2001.
- BANKER, B. Q.; LARROCHE, J. C. (1962): Periventricular leukomalacia of infancy. A form of neonatal anoxic encephalopathy. In *Arch Neurol* 7 (5), pp. 386–410. DOI: 10.1001/archneur.1962.04210050022004.
- Barnett, Madeleine L.; Tusor, Nora; Ball, Gareth; Chew, Andrew; Falconer, Shona; Aljabar, Paul et al. (2018): Exploring the multiple-hit hypothesis of preterm white matter damage using diffusion MRI. In *NeuroImage. Clinical* 17, pp. 596–606. DOI: 10.1016/j.nicl.2017.11.017.
- Batalle, Dafnis; Hughes, Emer J.; Zhang, Hui; Tournier, J-Donald; Tusor, Nora; Aljabar, Paul et al. (2017): Early development of structural networks and the impact of prematurity on brain connectivity. In *NeuroImage* 149, pp. 379–392. DOI: 10.1016/j.neuroimage.2017.01.065.
- Bäumli, Josef G.; Daamen, Marcel; Meng, Chun; Neitzel, Julia; Scheef, Lukas; Jaekel, Julia et al. (2015): Correspondence Between Aberrant Intrinsic Network Connectivity and Gray-Matter Volume in the Ventral Brain of Preterm Born Adults. In *Cerebral cortex (New York, N.Y. : 1991)* 25 (11), pp. 4135–4145. DOI: 10.1093/cercor/bhu133.
- Benjamini, Yoav; Hochberg, Yosef (1995): Controlling the False Discovery Rate: A Practical and Powerful Approach to Multiple Testing. In *Journal of the Royal Statistical Society: Series B (Methodological)* 57 (1), pp. 289–300. DOI: 10.1111/j.2517-6161.1995.tb02031.x.
- Billiards, Saraid S.; Haynes, Robin L.; Folkerth, Rebecca D.; Borenstein, Natalia S.; Trachtenberg, Felicia L.; Rowitch, David H. et al. (2008): Myelin abnormalities without oligodendrocyte loss in periventricular leukomalacia. In *undefined* 18 (2), pp. 153–163. DOI: 10.1111/j.1750-3639.2007.00107.x.

Billiards, Saraid S.; Haynes, Robin L.; Folkerth, Rebecca D.; Trachtenberg, Felicia L.; Liu, Lena G.; Volpe, Joseph J.; Kinney, Hannah C. (2006): Development of microglia in the cerebral white matter of the human fetus and infant. In *J. Comp. Neurol.* 497 (2), pp. 199–208. DOI: 10.1002/cne.20991.

Boardman, J. P.; Craven, C.; Valappil, S.; Counsell, S. J.; Dyet, L. E.; Rueckert, D. et al. (2010): A common neonatal image phenotype predicts adverse neurodevelopmental outcome in children born preterm. In *NeuroImage* 52 (2), pp. 409–414. DOI: 10.1016/j.neuroimage.2010.04.261.

Box, George E.P.; Tiao, George C. (1992): Bayesian Inference in Statistical Analysis. Hoboken, NJ, USA: John Wiley & Sons, Inc.

Buntinx, Mieke; Moreels, Marjan; Vandenabeele, Frank; Lambrechts, Ivo; Raus, Jef; Steels, Paul et al. (2004): Cytokine-induced cell death in human oligodendroglial cell lines: I. Synergistic effects of IFN-gamma and TNF-alpha on apoptosis. In *Journal of neuroscience research* 76 (6), pp. 834–845. DOI: 10.1002/jnr.20118.

Buser, Joshua R.; Maire, Jennifer; Riddle, Art; Gong, Xi; Nguyen, Thuan; Nelson, Kerst et al. (2012): Arrested preoligodendrocyte maturation contributes to myelination failure in premature infants. In *Annals of neurology* 71 (1), pp. 93–109. DOI: 10.1002/ana.22627.

Bystron, Irina; Blakemore, Colin; Rakic, Pasko (2008): Development of the human cerebral cortex: Boulder Committee revisited. In *Nat Rev Neurosci* 9 (2), pp. 110–122. DOI: 10.1038/nrn2252.

Cai, T. Tony; Ma, Zongming; Wu, Yihong (2013): Sparse PCA: Optimal rates and adaptive estimation. In *aos* 41 (6), pp. 3074–3110. DOI: 10.1214/13-AOS1178.

Chen, Yachi; Ghosh, Anirvan (2005): Regulation of dendritic development by neuronal activity. In *Journal of Neurobiology* 64 (1), pp. 4–10. DOI: 10.1002/neu.20150.

Cho, Woo-Hyun; Barcelon, Ellane; Lee, Sung Joong (2016): Optogenetic Glia Manipulation: Possibilities and Future Prospects. In *Experimental Neurobiology* 25 (5), pp. 197–204. DOI: 10.5607/en.2016.25.5.197.

Cohen, Jacob (2013): Statistical Power Analysis for the Behavioral Sciences: Academic Press.

David Smith, A.; Paul Bolam, J. (1990): The neural network of the basal ganglia as revealed by the study of synaptic connections of identified neurones. In *Trends in Neurosciences* 13 (7), pp. 259–265. DOI: 10.1016/0166-2236(90)90106-k.

Dean, Justin M.; McClendon, Evelyn; Hansen, Kelly; Azimi-Zonooz, Aryan; Chen, Kevin; Riddle, Art et al. (2013): Prenatal cerebral ischemia disrupts MRI-defined cortical microstructure through disturbances in neuronal arborization. In *Science translational medicine* 5 (168), 168ra7. DOI: 10.1126/scitranslmed.3004669.

Desikan, Rahul S.; Ségonne, Florent; Fischl, Bruce; Quinn, Brian T.; Dickerson, Bradford C.; Blacker, Deborah et al. (2006): An automated labeling system for subdividing the human cerebral cortex on MRI scans into gyral based regions of interest. In *NeuroImage* 31 (3), pp. 968–980. DOI: 10.1016/j.neuroimage.2006.01.021.

Eikenes, Live; Løhaugen, Gro C.; Brubakk, Ann-Mari; Skranes, Jon; Håberg, Asta K. (2011): Young adults born preterm with very low birth weight demonstrate widespread white matter alterations on brain DTI. In *NeuroImage* 54 (3), pp. 1774–1785. DOI: 10.1016/j.neuroimage.2010.10.037.

Fischl, Bruce (2012): FreeSurfer. In *NeuroImage* 62 (2), pp. 774–781. DOI: 10.1016/j.neuroimage.2012.01.021.

- Groenewegen, Henk J. (2003): The basal ganglia and motor control. In *Neural Plasticity* 10 (1-2), pp. 107–120. DOI: 10.1155/NP.2003.107.
- Grothe, Michel J.; Scheef, Lukas; Bäuml, Josef; Meng, Chun; Daamen, Marcel; Baumann, Nicole et al. (2017): Reduced Cholinergic Basal Forebrain Integrity Links Neonatal Complications and Adult Cognitive Deficits After Premature Birth. In *Biological Psychiatry* 82 (2), pp. 119–126. DOI: 10.1016/j.biopsych.2016.12.008.
- Hammond, Timothy R.; Dufort, Connor; Dissing-Olesen, Lasse; Giera, Stefanie; Young, Adam; Wysoker, Alec et al. (2019): Single-Cell RNA Sequencing of Microglia throughout the Mouse Lifespan and in the Injured Brain Reveals Complex Cell-State Changes. In *Immunity* 50 (1), 253-271.e6. DOI: 10.1016/j.immuni.2018.11.004.
- Hammond, Timothy R.; Robinton, Daisy; Stevens, Beth (2018): Microglia and the Brain: Complementary Partners in Development and Disease. In *Annu. Rev. Cell Dev. Biol.* 34 (1), pp. 523–544. DOI: 10.1146/annurev-cellbio-100616-060509.
- Haynes, Robin L.; Borenstein, Natalia S.; Desilva, Tara M.; Folkerth, Rebecca D.; Liu, Lena G.; Volpe, Joseph J.; Kinney, Hannah C. (2005): Axonal development in the cerebral white matter of the human fetus and infant. In *J. Comp. Neurol.* 484 (2), pp. 156–167. DOI: 10.1002/cne.20453.
- Haynes, Robin L.; Folkerth, Rebecca D.; Keefe, Rachael J.; Sung, Iyue; Swzeda, Luke I.; Rosenberg, Paul A. et al. (2003): Nitrosative and oxidative injury to premyelinating oligodendrocytes in periventricular leukomalacia. In *J Neuropathol Exp Neurol* 62 (5), pp. 441–450. DOI: 10.1093/jnen/62.5.441.
- Hedderich, Dennis M.; Avram, Mihai; Menegaux, Aurore; Nuttall, Rachel; Zimmermann, Juliana; Schneider, Sebastian C. et al. (2020a): Hippocampal subfield volumes are nonspecifically reduced in premature-born adults. In *Human Brain Mapping* 41 (18), pp. 5215–5227. DOI: 10.1002/hbm.25187.
- Hedderich, Dennis M.; Bäuml, Josef G.; Berndt, Maria T.; Menegaux, Aurore; Scheef, Lukas; Daamen, Marcel et al. (2019): Aberrant gyrification contributes to the link between gestational age and adult IQ after premature birth. In *Brain* 142 (5), pp. 1255–1269. DOI: 10.1093/brain/awz071.
- Hedderich, Dennis M.; Bäuml, Josef G.; Menegaux, Aurore; Avram, Mihai; Daamen, Marcel; Zimmer, Claus et al. (2020b): An analysis of MRI derived cortical complexity in premature-born adults: Regional patterns, risk factors, and potential significance. In *NeuroImage* 208, p. 116438. DOI: 10.1016/j.neuroimage.2019.116438.
- Hedderich, Dennis M.; Boeckh-Behrens, Tobias; Bäuml, Josef G.; Menegaux, Aurore; Daamen, Marcel; Zimmer, Claus et al. (2020c): Sequelae of Premature Birth in Young Adults : Incidental Findings on Routine Brain MRI. In *Clin Neuroradiol*, pp. 1–9. DOI: 10.1007/s00062-020-00901-6.
- Hernán, M. A.; Robins, J. M. (2020): *Causal Inference: What If.*: Boca Raton: Chapman & Hall/CRC.
- Hickman, Suzanne; Izzy, Saef; Sen, Pritha; Morsett, Liza; El Khoury, Joseph (2018): Microglia in neurodegeneration. In *Nat Neurosci* 21 (10), pp. 1359–1369. DOI: 10.1038/s41593-018-0242-x.
- Jenkinson, Mark; Beckmann, Christian F.; Behrens, Timothy E. J.; Woolrich, Mark W.; Smith, Stephen M. (2012): FSL. In *NeuroImage* 62 (2), pp. 782–790. DOI: 10.1016/j.neuroimage.2011.09.015.
- Kemp, J. M.; Powell, T. P. (1971): The connexions of the striatum and globus pallidus: synthesis and speculation. In *Philosophical transactions of the Royal Society of London. Series B, Biological sciences* 262 (845), pp. 441–457. DOI: 10.1098/rstb.1971.0106.
- Kinney, Hannah C.; Haynes, Robin L.; Xu, Gang; Andiman, Sarah E.; Folkerth, Rebecca D.; Sleeper, Lynn A.; Volpe, Joseph J. (2012): Neuron deficit in the white matter and subplate in periventricular leukomalacia. In *Annals of neurology* 71 (3), pp. 397–406. DOI: 10.1002/ana.22612.

- Köhler, Stefanie; Bär, Karl-Jürgen; Wagner, Gerd (2016): Differential involvement of brainstem noradrenergic and midbrain dopaminergic nuclei in cognitive control. In *Human Brain Mapping* 37 (6), pp. 2305–2318. DOI: 10.1002/hbm.23173.
- Kostović, Ivica; Jovanov-Milosević, Natasa (2006): The development of cerebral connections during the first 20-45 weeks' gestation. In *Seminars in Fetal and Neonatal Medicine* 11 (6), pp. 415–422. DOI: 10.1016/j.siny.2006.07.001.
- Kostović, Ivica; Judas, Milos (2002): Correlation between the sequential ingrowth of afferents and transient patterns of cortical lamination in preterm infants. In *Anat. Rec.* 267 (1), pp. 1–6. DOI: 10.1002/ar.10069.
- Krout, Karl E.; Belzer, Rebecca E.; Loewy, Arthur D. (2002): Brainstem projections to midline and intralaminar thalamic nuclei of the rat. In *J. Comp. Neurol.* 448 (1), pp. 53–101. DOI: 10.1002/cne.10236.
- Letinic, Kresimir; Zoncu, Roberto; Rakic, Pasko (2002): Origin of GABAergic neurons in the human neocortex. In *Nature* 417 (6889), pp. 645–649. DOI: 10.1038/nature00779.
- Liddell, Belinda J.; Brown, Kerri J.; Kemp, Andrew H.; Barton, Matthew J.; Das, Pritha; Peduto, Anthony et al. (2005): A direct brainstem-amygdala-cortical 'alarm' system for subliminal signals of fear. In *NeuroImage* 24 (1), pp. 235–243. DOI: 10.1016/j.neuroimage.2004.08.016.
- Liddel, Shane A.; Barres, Ben A. (2017): Reactive Astrocytes: Production, Function, and Therapeutic Potential. In *Immunity* 46 (6), pp. 957–967. DOI: 10.1016/j.immuni.2017.06.006.
- Liddel, Shane A.; Guttenplan, Kevin A.; Clarke, Laura E.; Bennett, Frederick C.; Bohlen, Christopher J.; Schirmer, Lucas et al. (2017): Neurotoxic reactive astrocytes are induced by activated microglia. In *Nature* 541 (7638), pp. 481–487. DOI: 10.1038/nature21029.
- Loh, Wai Yen; Anderson, Peter J.; Cheong, Jeanie L. Y.; Spittle, Alicia J.; Chen, Jian; Lee, Katherine J. et al. (2017): Neonatal basal ganglia and thalamic volumes: very preterm birth and 7-year neurodevelopmental outcomes. In *Pediatr Res* 82 (6), pp. 970–978. DOI: 10.1038/pr.2017.161.
- Mann, H. B.; Whitney, D. R. (1947): On a Test of Whether one of Two Random Variables is Stochastically Larger than the Other. In *Ann. Math. Statist.* 18 (1), pp. 50–60. DOI: 10.1214/aoms/1177730491.
- Marinescu, Razvan V.; Eshaghi, Arman; Alexander, Daniel C.; Golland, Polina (2019): BrainPainter: A software for the visualisation of brain structures, biomarkers and associated pathological processes. In *arXiv preprint arXiv:1905.08627*.
- Mayo Clinic (2021a): Premature birth - Diagnosis and treatment - Mayo Clinic. Available online at <https://www.mayoclinic.org/diseases-conditions/premature-birth/diagnosis-treatment/drc-20376736>, updated on 8/31/2021, checked on 8/31/2021.
- Mayo Clinic (2021b): Premature birth - Symptoms and causes. Available online at <https://www.mayoclinic.org/diseases-conditions/premature-birth/symptoms-causes/syc-20376730>, updated on 8/31/2021, checked on 8/31/2021.
- McClendon, Evelyn; Chen, Kevin; Gong, Xi; Sharifnia, Elica; Hagen, Matthew; Cai, Victor et al. (2014): Prenatal cerebral ischemia triggers dysmaturation of caudate projection neurons. In *Annals of neurology* 75 (4), pp. 508–524. DOI: 10.1002/ana.24100.
- McQuillen, Patrick S.; Sheldon, R. Ann; Shatz, Carla J.; Ferriero, Donna M. (2003): Selective Vulnerability of Subplate Neurons after Early Neonatal Hypoxia-Ischemia. In *J. Neurosci.* 23 (8), pp. 3308–3315. DOI: 10.1523/JNEUROSCI.23-08-03308.2003.

Menegaux, Aurore; Hedderich, Dennis M.; Bäuml, Josef G.; Manoliu, Andrei; Daamen, Marcel; Berg, Ronja C. et al. (2020): Reduced apparent fiber density in the white matter of premature-born adults. In *Scientific reports* 10 (1), p. 17214. DOI: 10.1038/s41598-020-73717-6.

Menegaux, Aurore; Meng, Chun; Bäuml, Josef G.; Berndt, Maria T.; Hedderich, Dennis M.; Schmitz-Koep, Benita et al. (2021): Aberrant cortico-thalamic structural connectivity in premature-born adults. In *Cortex*. DOI: 10.1016/j.cortex.2021.04.009.

Meng, C.; Bäuml, J. G.; Daamen, M.; Jaekel, J.; Neitzel, J.; Scheef, L. et al. (2016): Extensive and interrelated subcortical white and gray matter alterations in preterm-born adults. In *Brain structure & function* 221 (4), pp. 2109–2121. DOI: 10.1007/s00429-015-1032-9.

Michell-Robinson, Mackenzie A.; Touil, Hanane; Healy, Luke M.; Owen, David R.; Durafourt, Bryce A.; Bar-Or, Amit et al. (2015): Roles of microglia in brain development, tissue maintenance and repair. In *Brain : a journal of neurology* 138 (Pt 5), pp. 1138–1159. DOI: 10.1093/brain/awv066.

Miron, Veronique E.; Boyd, Amanda; Zhao, Jing-Wei; Yuen, Tracy J.; Ruckh, Julia M.; Shadrach, Jennifer L. et al. (2013): M2 microglia and macrophages drive oligodendrocyte differentiation during CNS remyelination. In *Nat Neurosci* 16 (9), pp. 1211–1218. DOI: 10.1038/nn.3469.

Mori, Susumu; Wakana, S.; van Zijl, Peter C. M.; Nagae-Poetscher, L. M. (2005): MRI Atlas of Human White Matter: Elsevier.

Murtagh, Fionn; Contreras, Pedro (2012): Algorithms for hierarchical clustering: an overview. In *Wiley Interdisciplinary Reviews: Data Mining and Knowledge Discovery* 2 (1), pp. 86–97. DOI: 10.1002/widm.53.

Nosarti, Chiara; Nam, Kie Woo; Walshe, Muriel; Murray, Robin M.; Cuddy, Marion; Rifkin, Larry; Allin, Matthew P. G. (2014): Preterm birth and structural brain alterations in early adulthood. In *NeuroImage. Clinical* 6, pp. 180–191. DOI: 10.1016/j.nicl.2014.08.005.

Okoshi, Yumi; Itoh, Masayuki; Takashima, Sachio (2001): Characteristic neuropathology and plasticity in periventricular leukomalacia. In *Pediatric Neurology* 25 (3), pp. 221–226. DOI: 10.1016/S0887-8994(01)00309-5.

Pearl, Judea (2000): Models, reasoning and inference. 19th ed. Cambridge, UK: CambridgeUniversityPress.

Pediatric nurse (2021): Treatment of preterm born neonates and communication with their parents. Interview, 9/13/2021.

Pedregosa, F.; Varoquaux, G.; Gramfort, A.; Michel, V.; Thirion, B.; Grisel, O. et al. (2011): Scikit-learn: Machine learning in Python. In *Journal of Machine Learning Research* (12), 2825--2830.

Pierson, Christopher R.; Folkerth, Rebecca D.; Billiards, Saraïd S.; Trachtenberg, Felicia L.; Drinkwater, Mark E.; Volpe, Joseph J.; Kinney, Hannah C. (2007): Gray matter injury associated with periventricular leukomalacia in the premature infant. In *Acta Neuropathol* 114 (6), pp. 619–631. DOI: 10.1007/s00401-007-0295-5.

Pölsterl, Sebastian; Wachinger, Christian (2021): Estimation of Causal Effects in the Presence of Unobserved Confounding in the Alzheimer's Continuum. In Aasa Feragen, Stefan Sommer, Julia Schnabel, Mads Nielsen (Eds.): Information Processing in Medical Imaging, vol. 12729. Cham: Springer International Publishing (Lecture Notes in Computer Science), pp. 45–57.

Rangarajan, Vijayeta; Juul, Sandra E. (2014): Erythropoietin: emerging role of erythropoietin in neonatal neuroprotection. In *Pediatric Neurology* 51 (4), pp. 481–488. DOI: 10.1016/j.pediatrneurol.2014.06.008.

- Reemst, Kitty; Noctor, Stephen C.; Lucassen, Paul J.; Hol, Elly M. (2016): The Indispensable Roles of Microglia and Astrocytes during Brain Development. In *Front. Hum. Neurosci.* 10, p. 566. DOI: 10.3389/fnhum.2016.00566.
- Riddell, Allen; Hartikainen, Ari; Carter, Matthew (2021): PyStan. Version 3.0.0. PyPI. Available online at <https://pypi.org/project/pystan>.
- Robinson, Shenandoah; Li, Qing; Dechant, Anne; Cohen, Mark L. (2006): Neonatal loss of gamma-aminobutyric acid pathway expression after human perinatal brain injury. In *Journal of neurosurgery* 104 (6 Suppl), pp. 396–408. DOI: 10.3171/ped.2006.104.6.396.
- Ronan, Lisa; Voets, Natalie; Rua, Catarina; Alexander-Bloch, Aaron; Hough, Morgan; Mackay, Clare et al. (2014): Differential tangential expansion as a mechanism for cortical gyrification. In *Cerebral cortex (New York, N.Y. : 1991)* 24 (8), pp. 2219–2228. DOI: 10.1093/cercor/bht082.
- Sarnat, Harvey B.; Flores-Sarnat, Laura; Trevenen, Cynthia L. (2010): Synaptophysin immunoreactivity in the human hippocampus and neocortex from 6 to 41 weeks of gestation. In *J Neuropathol Exp Neurol* 69 (3), pp. 234–245. DOI: 10.1097/NEN.0b013e3181d0151f.
- Scafidi, Joseph; Hammond, Timothy R.; Scafidi, Susanna; Ritter, Jonathan; Jablonska, Beata; Roncal, Maria et al. (2014): Intranasal epidermal growth factor treatment rescues neonatal brain injury. In *Nature* 506 (7487), pp. 230–234. DOI: 10.1038/nature12880.
- Schaefer, Alexandre; Gray, Jeremy R. (2007): A role for the human amygdala in higher cognition. In *Reviews in the Neurosciences* 18 (5), pp. 355–363. DOI: 10.1515/revneuro.2007.18.5.355.
- Schafer, Dorothy P.; Lehrman, Emily K.; Kautzman, Amanda G.; Koyama, Ryuta; Mardinly, Alan R.; Yamasaki, Ryo et al. (2012): Microglia sculpt postnatal neural circuits in an activity and complement-dependent manner. In *Neuron* 74 (4), pp. 691–705. DOI: 10.1016/j.neuron.2012.03.026.
- Schmitz-Koep, Benita; Bäuml, Josef G.; Menegaux, Aurore; Nuttall, Rachel; Zimmermann, Juliana; Schneider, Sebastian C. et al. (2020): Decreased cortical thickness mediates the relationship between premature birth and cognitive performance in adulthood. In *Human Brain Mapping* 41 (17), pp. 4952–4963. DOI: 10.1002/hbm.25172.
- Schmitz-Koep, Benita; Zimmermann, Juliana; Menegaux, Aurore; Nuttall, Rachel; Bäuml, Josef G.; Schneider, Sebastian C. et al. (2021): Decreased amygdala volume in adults after premature birth. In *Scientific reports* 11 (1), p. 5403. DOI: 10.1038/s41598-021-84906-2.
- Seabold, Skipper; Perktold, Josef (2010): statsmodels: Econometric and statistical modeling with python. Proceedings of the 9th Python in Science Conference. Available online at <http://conference.scipy.org/proceedings/scipy2010/pdfs/seabold.pdf>.
- Semba, Kazue (1991): The Cholinergic Basal Forebrain: A Critical Role in Cortical Arousal. In T. Celeste Napier, Peter W. Kalivas, Israel Hanin (Eds.): *The Basal Forebrain: Anatomy to Function*. Boston, MA: Springer US, pp. 197–218.
- Shattuck, David W.; Leahy, Richard M. (2002): BrainSuite: An automated cortical surface identification tool. In *Medical Image Analysis* 6 (2), pp. 129–142. DOI: 10.1016/s1361-8415(02)00054-3.
- Shohamy, Daphna; Myers, Catherine E.; Hopkins, Ramona O.; Sage, Jake; Gluck, Mark A. (2009): Distinct hippocampal and basal ganglia contributions to probabilistic learning and reversal. In *Journal of Cognitive Neuroscience* 21 (9), pp. 1821–1833. DOI: 10.1162/jocn.2009.21138.
- Shuman, R. M.; Selednik, L. J. (1980): Periventricular leukomalacia. A one-year autopsy study. In *Arch Neurol* 37 (4), pp. 231–235. DOI: 10.1001/archneur.1980.00500530069011.

- Siglidis, Giannis; Nikolentzos, Giannis; Limnios, Stratis; Giatsidis, Christos; Skianis, Konstantinos; Vazirgiannis, Michalis (2020): GraKeL: A Graph Kernel Library in Python. Available online at <https://www.jmlr.org/papers/volume21/18-370/18-370.pdf>.
- Skranes, Jon; Løhaugen, Gro C. C.; Martinussen, Marit; Håberg, Asta; Brubakk, Ann-Mari; Dale, Anders M. (2013): Cortical surface area and IQ in very-low-birth-weight (VLBW) young adults. In *Cortex* 49 (8), pp. 2264–2271. DOI: 10.1016/j.cortex.2013.06.001.
- Squarzoni, Paola; Oller, Guillaume; Hoeffel, Guillaume; Pont-Lezica, Lorena; Rostaing, Philippe; Low, Donovan et al. (2014): Microglia modulate wiring of the embryonic forebrain. In *Cell Reports* 8 (5), pp. 1271–1279. DOI: 10.1016/j.celrep.2014.07.042.
- Stiles, Joan; Jernigan, Terry L. (2010): The basics of brain development. In *Neuropsychology review* 20 (4), pp. 327–348. DOI: 10.1007/s11065-010-9148-4.
- Tim Henderson (2021): timtadh/zhang-shasha: Tree edit distance using the Zhang Shasha algorithm. GitHub. Available online at <https://github.com/timtadh/zhang-shasha>, updated on 9/15/2021, checked on 9/15/2021.
- Tipping, Michael E.; Bishop, Christopher M. (1999): Probabilistic Principal Component Analysis. In *J Royal Statistical Soc B* 61 (3), pp. 611–622. DOI: 10.1111/1467-9868.00196.
- Titomanlio, Luigi; Kavelaars, Annemieke; Dalous, Jeremie; Mani, Shyamala; El Ghouzzi, Vincent; Heijnen, Cobi et al. (2011): Stem cell therapy for neonatal brain injury: perspectives and challenges. In *Annals of neurology* 70 (5), pp. 698–712. DOI: 10.1002/ana.22518.
- Tournier, J-Donald; Smith, Robert; Raffelt, David; Tabbara, Rami; Dhollander, Thijs; Pietsch, Maximilian et al. (2019): MRtrix3 : A fast, flexible and open software framework for medical image processing and visualisation: Cold Spring Harbor Laboratory.
- Vallat, Raphael (2018): Pingouin: statistics in Python. In *JOSS* 3 (31), p. 1026.
- van Rossum, Guido; Drake, Fred L. (2010): The Python language reference. Release 3.0.1 [Repr.]. Hampton, NH, Redwood City, Calif.: Python Software Foundation; SoHo Books (Documentation for Python, / Guido van Rossum; Fred L. Drake ed. ; Pt. 2).
- Virtanen, Pauli; Gommers, Ralf; Oliphant, Travis E.; Haberland, Matt; Reddy, Tyler; Cournapeau, David et al. (2020): SciPy 1.0: fundamental algorithms for scientific computing in Python. In *Nature methods* 17 (3), pp. 261–272. DOI: 10.1038/s41592-019-0686-2.
- Volpe, Joseph J. (2009): The encephalopathy of prematurity--brain injury and impaired brain development inextricably intertwined. In *Seminars in Pediatric Neurology* 16 (4), pp. 167–178. DOI: 10.1016/j.spn.2009.09.005.
- Volpe, Joseph J. (2019): Dysmaturational of Premature Brain: Importance, Cellular Mechanisms, and Potential Interventions. In *Pediatric Neurology* 95, pp. 42–66. DOI: 10.1016/j.pediatrneurol.2019.02.016.
- Volpe, Joseph J.; Kinney, Hannah C.; Jensen, Frances E.; Rosenberg, Paul A. (2011): The developing oligodendrocyte: key cellular target in brain injury in the premature infant. In *Int. j. dev. neurosci.* 29 (4), pp. 423–440. DOI: 10.1016/j.ijdevneu.2011.02.012.
- Wang, Yixin; Blei, David M. (2019): The Blessings of Multiple Causes. In *Journal of the American Statistical Association* 114 (528), pp. 1574–1596. DOI: 10.1080/01621459.2019.1686987.
- Waskom, Michael (2021): seaborn: statistical data visualization. In *JOSS* 6 (60), p. 3021. DOI: 10.21105/joss.03021.

White, Thomas P.; Symington, Iona; Castellanos, Nazareth P.; Brittain, Philip J.; Froudish Walsh, Seán; Nam, Kie-Woo et al. (2014): Dysconnectivity of neurocognitive networks at rest in very-preterm born adults. In *NeuroImage. Clinical* 4, pp. 352–365. DOI: 10.1016/j.nicl.2014.01.005.

WHO (2021): Preterm birth. Available online at <https://www.who.int/news-room/factsheets/detail/preterm-birth>, updated on 8/30/2021, checked on 8/31/2021.

Wolke, D.; Meyer, R. (1999): Cognitive status, language attainment, and prereading skills of 6-year-old very preterm children and their peers: the Bavarian Longitudinal Study. In *Developmental Medicine and Child Neurology* 41 (2), pp. 94–109. DOI: 10.1017/S0012162299000201.

Woodward, Lianne J.; Anderson, Peter J.; Austin, Nicola C.; Howard, Kelly; Inder, Terrie E. (2006): Neonatal MRI to predict neurodevelopmental outcomes in preterm infants. In *N Engl J Med* 355 (7), pp. 685–694. DOI: 10.1056/NEJMoa053792.

Xu, Gang; Broadbelt, Kevin G.; Haynes, Robin L.; Folkerth, Rebecca D.; Borenstein, Natalia S.; Belliveau, Richard A. et al. (2011): Late development of the GABAergic system in the human cerebral cortex and white matter. In *J Neuropathol Exp Neurol* 70 (10), pp. 841–858. DOI: 10.1097/NEN.0b013e31822f471c.

yWorks GmbH (2019): yEd. Version 3.19: yWorks GmbH. Available online at <https://www.yworks.com/products/yed>.

Zhang, Kaizhong; Shasha, Dennis (1989): Simple Fast Algorithms for the Editing Distance between Trees and Related Problems. In *SIAM J. Comput.* 18 (6), pp. 1245–1262. DOI: 10.1137/0218082.

Zhang, Yuning; Inder, Terrie E.; Neil, Jeffrey J.; Dierker, Donna L.; Alexopoulos, Dimitrios; Anderson, Peter J.; van Essen, David C. (2015): Cortical structural abnormalities in very preterm children at 7 years of age. In *NeuroImage* 109, pp. 469–479. DOI: 10.1016/j.neuroimage.2015.01.005.

9 Appendix

9.1 P-values and effect sizes for significance analysis

In this table, corrected p-values as well as effect sizes are displayed for the comparison VP/VLBW group and FT group. The values are sorted by ascending corrected p-value and labels are according to the extraction from Freesurfer, localGI is short for local gyrification index.

Variables	p_value_corrected	cohens_d
Left-Thalamus	5.34E-13	1.31443
Right-Thalamus	5.34E-13	1.282291
R_transversetemporal_localGI	1.8E-11	1.204942
R_superiortemporal_localGI	1.77E-09	1.03354
L_transversetemporal_localGI	2.21E-09	1.041901
Brain-Stem	2.93E-09	1.01988
Right-Hippocampus	3.23E-09	1.052627
R_insula_localGI	4.59E-09	1.036773
Left-Hippocampus	6.58E-09	0.995734
rh_middletemporal_volume	7.76E-09	0.973433
R_parsopercularis_localGI	8.64E-09	0.99812
Right-Accumbens-area	2.61E-08	0.929238
Left-Caudate	3.94E-08	0.954685

Right-Caudate	4.69E-08	0.881549
Left-Accumbens-area	1.17E-07	0.879766
L_superiortemporal_localGI	4.57E-07	0.851084
L_insula_localGI	1.03E-06	0.824676
R_superiorparietal_localGI	1.03E-06	0.778709
R_middletemporal_localGI	1.69E-06	0.767988
Left-Pallidum	2.2E-06	0.799583
R_parstriangularis_localGI	3.32E-06	0.782315
lh_middletemporal_volume	4.09E-06	0.755928
rh_isthmuscingulate_volume	1.14E-05	0.761077
fd_Body_CC	2.83E-05	0.822217
rh_lateralorbitofrontal_volume	2.83E-05	0.67475
fa_Ext_caps_L	3.06E-05	0.864511
lh_parsorbitalis_volume	4.38E-05	0.679937
fa_Fornix	4.8E-05	0.839191
InSituTot	5.16E-05	0.700548
L_parsopercularis_localGI	5.2E-05	0.676706
L_cuneus_localGI	6.35E-05	0.712247
fa_Cingulum_R	8.34E-05	0.795285
Right-Pallidum	9.26E-05	0.658212
fd_Fornix_strialis_L	0.000125	0.778143
L_middletemporal_localGI	0.000125	0.643475
L_precuneus_localGI	0.000152	0.626833
fa_Uncinate_R	0.000156	0.76734
lh_isthmuscingulate_volume	0.000161	0.609861
R_lateraloccipital_localGI	0.000167	0.621515
Left-Amygdala	0.000179	0.613205
fa_Fornix_stria_terminalis_L	0.000188	0.777673
R_parsorbitalis_localGI	0.00019	0.643809
rh_supramarginal_volume	0.000265	0.593456
fa_Ext_caps_R	0.000289	0.704547
L_pericalcarine_localGI	0.000303	0.610989
rh_bankssts_volume	0.000303	0.543177
rh_inferiorparietal_volume	0.000335	0.566753
R_precuneus_localGI	0.000336	0.494672
L_superiorparietal_localGI	0.000504	0.586429
lh_lateralorbitofrontal_volume	0.000578	0.579959
lh_inferiorparietal_volume	0.0007	0.580615
fa_Uncinate_L	0.00077	0.660685
R_postcentral_localGI	0.00077	0.555201
lh_precentral_volume	0.00077	0.524609
fd_Genu_CC	0.000773	0.672072
rh_posteriorcingulate_volume	0.000773	0.588391
R_cuneus_localGI	0.000803	0.495746
rhCerebralWhiteMatterVol	0.000969	0.591055
rh_rostralanteriorcingulate_volume	0.001032	0.516733
lhCerebralWhiteMatterVol	0.001066	0.566878

fa_Cingulum_L	0.001182	0.624498
rh_parsorbitalis_volume	0.001184	0.592678
Right-Putamen	0.001402	0.551671
lh_superiorparietal_volume	0.001611	0.549859
rh_superiorparietal_volume	0.001624	0.561458
Right-Amygdala	0.001654	0.551289
EstimatedTotalIntraCranialVol	0.001952	0.476516
lh_parstriangularis_volume	0.002132	0.488203
fd_Fornix	0.002174	0.679571
fa_Body_CC	0.002174	0.68388
rh_precentral_volume	0.002393	0.472054
fd_Cingulum_R	0.002956	0.654636
fa_Sup_cereb_ped_L	0.003417	0.612101
fd_Ext_caps_R	0.003433	0.499798
rh_postcentral_volume	0.003433	0.476652
fd_Cerebral_ped_R	0.003792	0.55578
fd_Fornix_strialis_R	0.003792	0.559008
R_pericalcarine_localGI	0.003792	0.456143
L_paracentral_localGI	0.004751	0.439554
fd_Uncinate_R	0.005387	0.513247
R_supramarginal_localGI	0.006008	0.395182
lh_bankssts_volume	0.006115	0.453703
R_precentral_localGI	0.006468	0.424207
lh_posteriorcingulate_volume	0.007534	0.463524
fa_Sup_cereb_ped_R	0.007741	0.58851
fa_Cerebral_ped_R	0.008368	0.535718
lh_postcentral_volume	0.008555	0.47302
fd_Sup_cereb_ped_R	0.008742	0.546687
lh_supramarginal_volume	0.009007	0.411488
fa_PTR_L	0.009034	0.450467
fd_Ext_caps_L	0.010531	0.569706
fd_Sup_cereb_ped_L	0.011359	0.522341
Right-Cerebellum-White-Matter	0.011962	0.405685
fd_Tapetum_L	0.012916	0.526545
rh_fusiform_volume	0.013293	0.379612
fa_Tapetum_L	0.013337	0.579798
L_lingual_localGI	0.014248	0.405009
Left-Putamen	0.016404	0.42723
rh_lingual_volume	0.016809	0.364714
Right-Cerebellum-Cortex	0.017225	0.376204
rh_precuneus_volume	0.018057	0.433327
fd_Splenium_CC	0.019006	0.513524
rh_transversetemporal_volume	0.019978	0.415103
L parahippocampal_localGI	0.022296	0.346879
rh_parstriangularis_volume	0.024216	0.397595
fa_Inf_cereb_ped_R	0.025427	0.435585
lh_rostralmiddlefrontal_volume	0.028805	0.33718

fd_Post_limb_IC_R	0.033655	0.405535
fd_Cingulum_L	0.033984	0.497395
lh_superiorfrontal_volume	0.037044	0.327787
fd_Ant_limb_IC_L	0.039869	0.413055
Left-Cerebellum-White-Matter	0.043953	0.345077
fd_Uncinate_L	0.044541	0.398506
lh_fusiform_volume	0.045432	0.356948
lh_lingual_volume	0.046112	0.331702
lh_rostralanteriorcingulate_volume	0.046959	0.380919
lh_cuneus_volume	0.049609	0.332458
rh_cuneus_volume	0.053253	0.23131
fd_Post_CR_R	0.053939	0.417985
lh_insula_volume	0.053939	0.30995
CC_Mid_Anterior	0.059946	0.356753
fa_Fornix_stria_terminalis_R	0.067665	0.368798
L_isthmuscingulate_localGI	0.067665	0.289069
L_parstriangularis_localGI	0.071713	0.280668
L_postcentral_localGI	0.078111	0.273811
fa_Genu_CC	0.080123	0.369424
L_precentral_localGI	0.080274	0.263693
CC_Anterior	0.08997	0.294658
lh_transversetemporal_volume	0.093949	0.322211
rh_insula_volume	0.097497	0.273518
fa_Ant_CR_L	0.09836	0.249064
CC_Central	0.100977	0.287855
R_lingual_localGI	0.120687	0.278986
Left-Cerebellum-Cortex	0.122903	0.260183
L_lateraloccipital_localGI	0.125505	0.34203
fa_SLF_R	0.129309	0.229539
L_posteriorcingulate_localGI	0.143028	0.219981
fd_Tapetum_R	0.144732	0.363785
fa_Tapetum_R	0.145861	0.354283
R_frontalpole_localGI	0.145861	0.275223
rh_caudalanteriorcingulate_volume	0.152518	0.235229
fa_Inf_cereb_ped_L	0.156992	0.310597
lh parahippocampal_volume	0.162597	0.14059
fd_Post_limb_IC_L	0.165183	0.330926
lh_parsopercularis_volume	0.168221	0.218853
fa_Cingulum_hippo_L	0.170041	0.237728
fa_Cingulum_hippo_R	0.171296	0.291092
R_lateralorbitofrontal_localGI	0.176475	0.267131
fd_CST_L	0.182403	0.28401
R_inferiortemporal_localGI	0.182403	0.205406
rh_superiorfrontal_volume	0.182403	0.239884
lh_medialorbitofrontal_volume	0.182403	0.218564
L_supramarginal_localGI	0.186891	0.156999
fa_SFOF_R	0.202669	0.18399

CC_Posterior	0.209275	0.099029
fa_Ant_CR_R	0.209275	0.231198
rh_entorhinal_volume	0.209275	0.245353
fa_PTR_R	0.222789	0.28092
lh_caudalmiddlefrontal_volume	0.223068	0.221872
fa_Post_limb_IC_R	0.230343	0.24928
fa_Retrolent_part_IC_L	0.231915	0.29902
L_inferiorparietal_localGI	0.237171	0.178494
fa_Retrolent_part_IC_R	0.239685	0.194643
rh_superiortemporal_volume	0.242257	0.180046
R_bankssts_localGI	0.245995	0.187377
fa_Mid_cereb_peduncle	0.250881	0.256849
fd_Cingulum_hippo_R	0.259002	0.221172
L_frontalpole_localGI	0.273691	0.17193
R_paracentral_localGI	0.273691	0.189075
rh_frontalpole_volume	0.27458	0.206015
fa_SFOF_L	0.291511	0.24465
rh_medialorbitofrontal_volume	0.292487	0.219583
L_fusiform_localGI	0.294736	0.218794
WM-hypointensities	0.295016	0.289361
lh_lateraloccipital_volume	0.298607	0.216568
fd_SFOF_R	0.298986	0.163861
Optic-Chiasm	0.305199	0.204625
R_rostralanteriorcingulate_localGI	0.308193	0.186166
fd_Medial_lemn_R	0.32118	0.136456
R_posteriorcingulate_localGI	0.322517	0.136091
rh parahippocampal_volume	0.325912	0.079598
lh_pericalcarine_volume	0.325912	0.150074
fd_SLF_L	0.342575	0.255314
rh_temporalpole_volume	0.342575	0.123712
fd_SFOF_L	0.372665	0.243408
L_rostralmiddlefrontal_localGI	0.37968	0.220232
rh_rostralmiddlefrontal_volume	0.37968	0.172142
L_temporalpole_localGI	0.381515	0.158241
fd_Sup_CR_R	0.383359	0.214392
fa_Cerebral_ped_L	0.383359	0.194037
R_isthmuscingulate_localGI	0.383359	0.067026
rh_pericalcarine_volume	0.394404	0.095132
fd_Ant_limb_IC_R	0.404617	0.171455
fa_Sag_stratum_R	0.404673	0.1993
lh_paracentral_volume	0.412829	0.160787
R_medialorbitofrontal_localGI	0.416367	0.141799
fd_Medial_lemn_L	0.420007	0.173295
lh_superiortemporal_volume	0.425115	0.131239
R_caudalmiddlefrontal_localGI	0.438624	0.16027
L_unknown	0.457473	0.063468
R_fusiform_localGI	0.457752	0.131332

fa_Sup_CR_R	0.465219	0.181605
R_inferiorparietal_localGI	0.469474	0.129901
rh_parsopercularis_volume	0.485442	0.103389
fd_CST_R	0.491052	0.118148
fd_Retrolent_part_IC_R	0.500606	0.064335
fa_CST_R	0.515112	0.068046
lh_precuneus_volume	0.52048	0.101896
R_unknown	0.535391	0.054831
L_superiorfrontal_localGI	0.553316	0.121784
lh_caudalanteriorcingulate_volume	0.561042	0.140338
fa_Post_CR_L	0.56142	0.136341
rh_paracentral_volume	0.56142	0.126262
lh_inferiortemporal_volume	0.561616	0.130386
fd_Pontine_crossing_tract	0.564359	0.11981
fd_PTR_R	0.569342	0.118107
fa_Post_limb_IC_L	0.579445	0.117387
fd_Mid_cereb_peduncle	0.589609	0.081829
fa_Sag_stratum_L	0.594523	0.02078
L_bankssts_localGI	0.594523	0.143156
R parahippocampal_localGI	0.606776	0.095497
fd_Cerebral_ped_L	0.63064	0.101168
R_superiorfrontal_localGI	0.63064	0.099271
L_caudalanteriorcingulate_localGI	0.642385	0.056019
fd_Sup_CR_L	0.646171	0.168975
fa_Ant_limb_IC_L	0.662008	0.109334
L_caudalmiddlefrontal_localGI	0.690721	0.068626
fd_Inf_cereb_ped_R	0.735601	0.14469
fa_CST_L	0.737822	0.126861
L_lateralorbitofrontal_localGI	0.737822	0.06141
rh_inferiortemporal_volume	0.737822	0.051274
fd_Ant_CR_L	0.750722	0.091752
lh_frontalpole_volume	0.754232	0.014844
fa_Medial_lemn_L	0.7606	0.070036
R_temporalpole_localGI	0.7606	0.055948
fa_Pontine_crossing_tract	0.76295	0.077117
fd_Inf_cereb_ped_L	0.768084	0.171143
L_entorhinal_localGI	0.772298	0.091501
lh_entorhinal_volume	0.790844	0.148836
fa_SLF_L	0.791806	0.08221
fa_Splenium_CC	0.802495	0.144805
fd_Cingulum_hippo_L	0.821613	0.08217
fd_PTR_L	0.828324	0.069912
L_rostralanteriorcingulate_localGI	0.828324	0.037032
fa_Medial_lemn_R	0.831098	0.058461
fd_Retrolent_part_IC_L	0.857912	0.010876
fd_Sag_stratum_L	0.857912	0.003978
L_parsorbitalis_localGI	0.860481	0.005853

fa_Sup_CR_L	0.876203	0.057829
R_rostralmiddlefrontal_localGI	0.879534	0.07101
fd_Sag_stratum_R	0.89594	0.011429
fd_SLF_R	0.89594	0.070227
rh_lateraloccipital_volume	0.89594	0.005946
R_caudalanteriorcingulate_localGI	0.909976	0.05789
fd_Ant_CR_R	0.910791	0.05331
CC_Mid_Posterior	0.929631	0.165592
fa_Ant_limb_IC_R	0.935983	0.052776
rh_caudalmiddlefrontal_volume	0.935983	0.028818
L_medialorbitofrontal_localGI	0.953007	0.02643
R_entorhinal_localGI	0.953007	0.023659
lh_temporalpole_volume	0.976836	0.141522
fd_Post_CR_L	0.978938	0.003454
fa_Post_CR_R	0.994272	0.006118
L_inferiortemporal_localGI	0.998992	0.015658

9.2 Pair plot

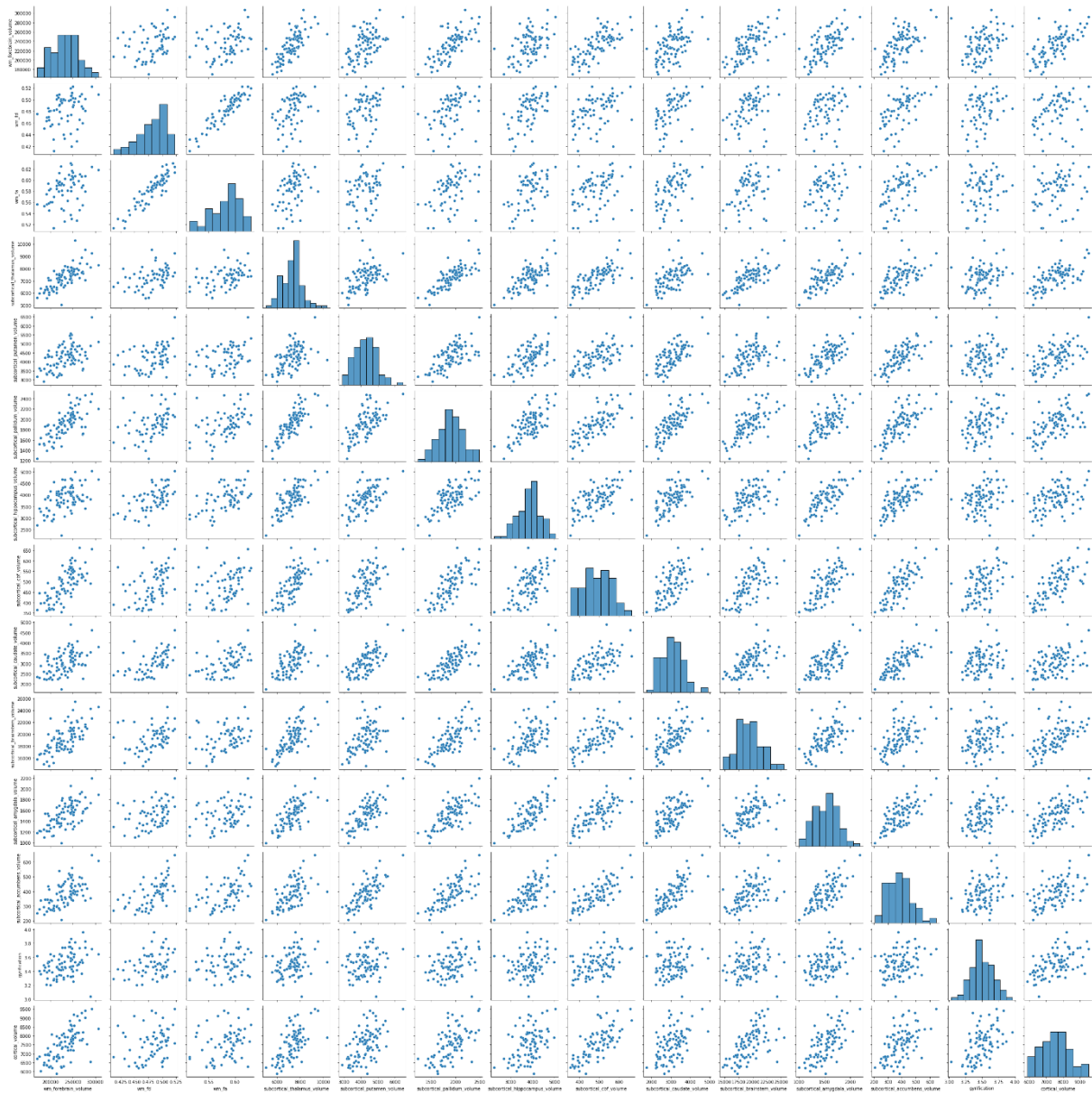


Figure 38 - Pair plot for the combinations of significantly different developmental processes

9.3 Histogram for the distribution of IQ

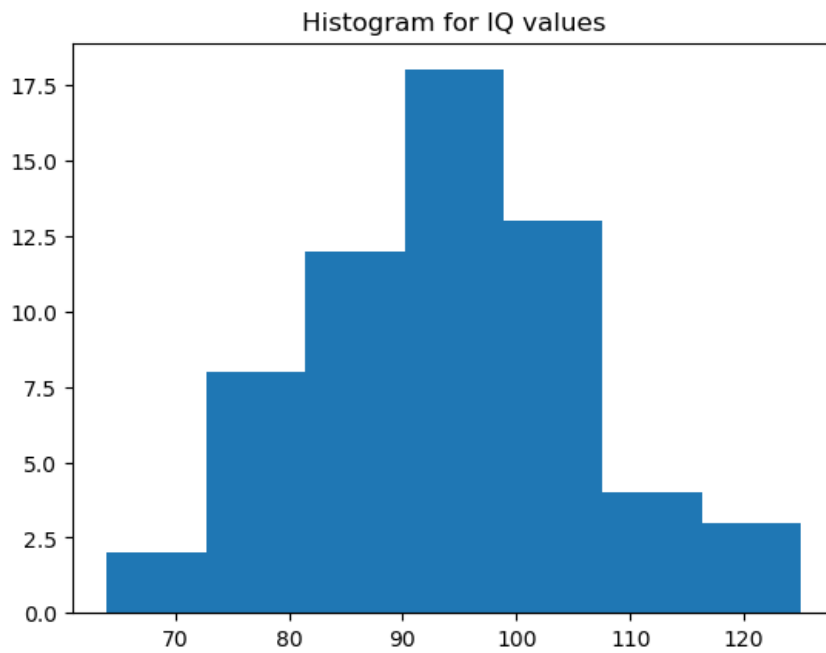


Figure 39 - Distribution of IQ scores

9.4 Effect sizes of non-causally significant developmental processes

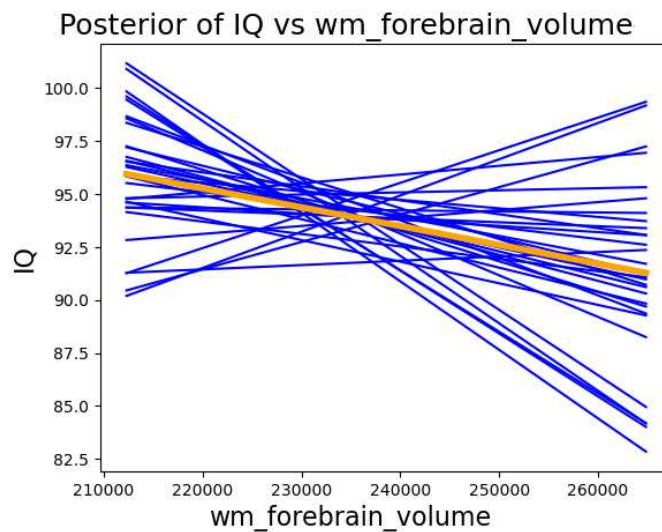


Figure 40 - Effect size of white matter forebrain volume on IQ, blue depicts predictions by drawing from the posterior distribution, orange depicts mean of predictions

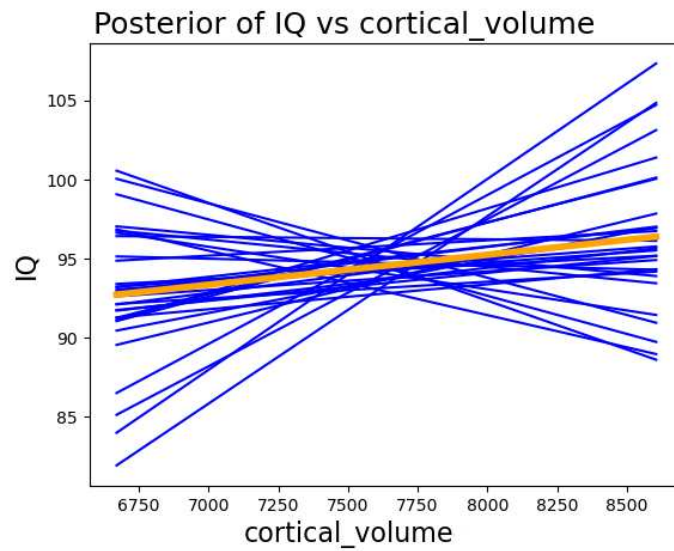


Figure 41 - Effect size of cortical volume on IQ, blue depicts predictions by drawing from the posterior distribution, orange depicts mean of predictions

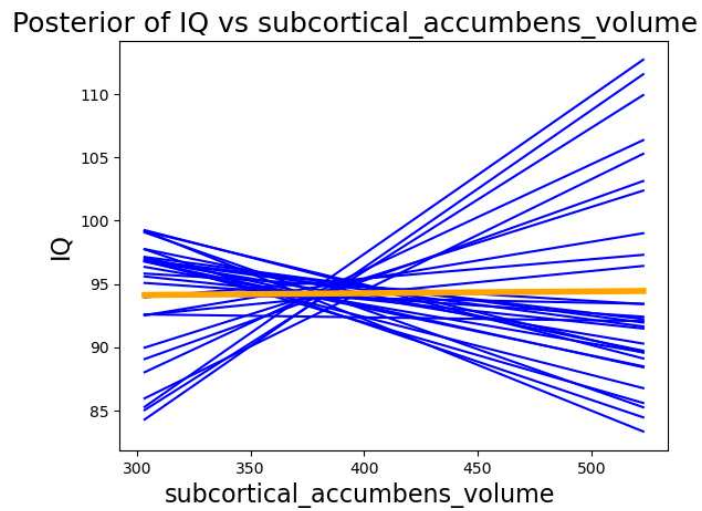


Figure 42 - Effect size of accumbens volume on IQ, blue depicts predictions by drawing from the posterior distribution, orange depicts mean of predictions

Posterior of IQ vs subcortical_caudate_volume

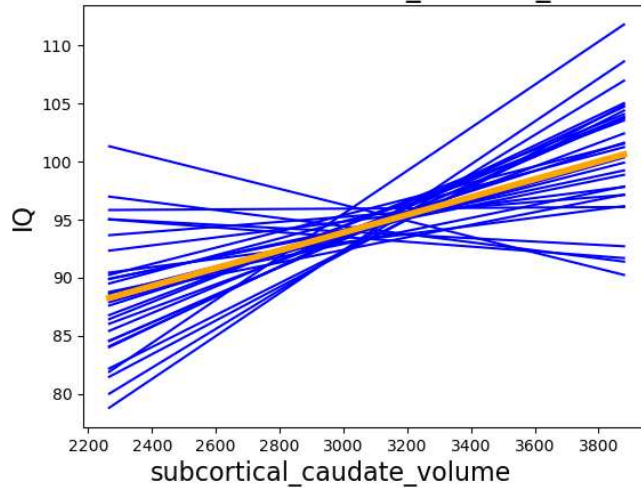


Figure 43 - Effect size of caudate volume on IQ, blue depicts predictions by drawing from the posterior distribution, orange depicts mean of predictions

Posterior of IQ vs subcortical_hippocampus_volume

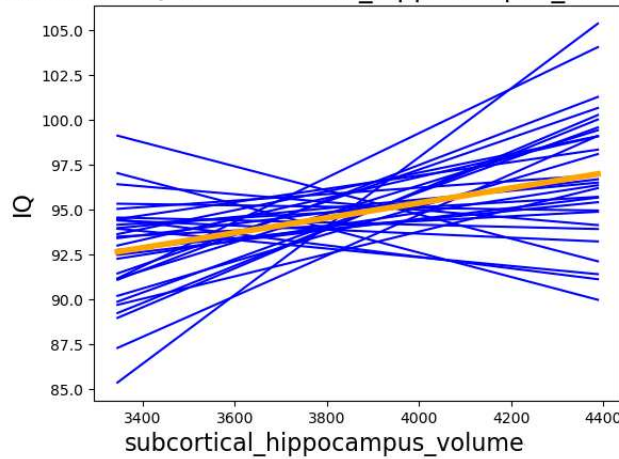


Figure 44 - Effect size of hippocampus volume on IQ, blue depicts predictions by drawing from the posterior distribution, orange depicts mean of predictions

Posterior of IQ vs subcortical_pallidum_volume

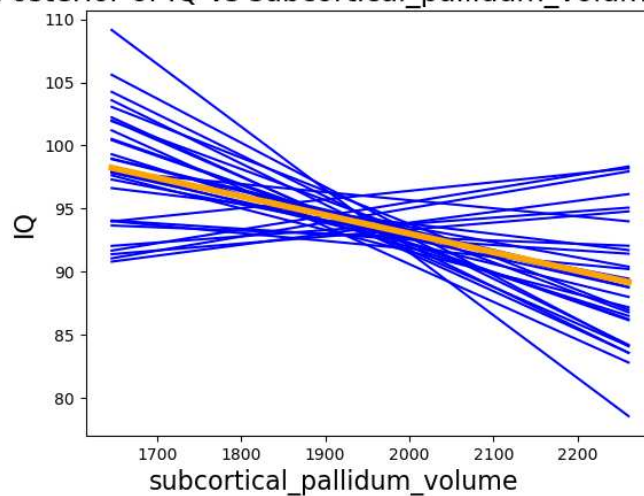


Figure 45 - Effect size of pallidum volume on IQ, blue depicts predictions by drawing from the posterior distribution, orange depicts mean of predictions

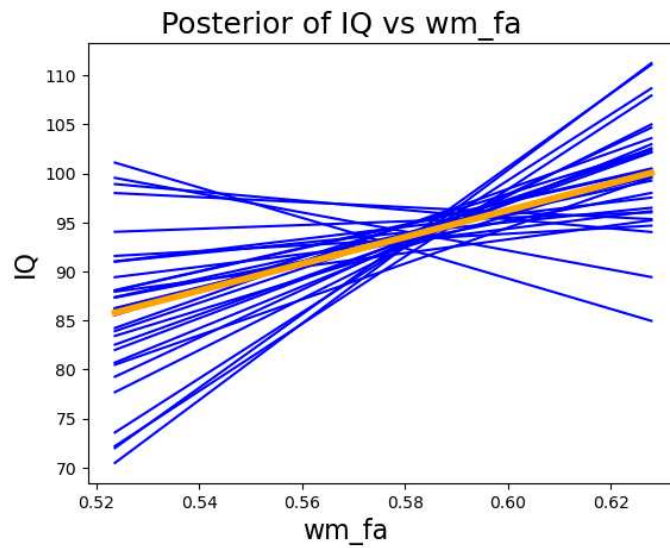


Figure 46 - Effect size of fractional anisotropy on IQ, blue depicts predictions by drawing from the posterior distribution, orange depicts mean of predictions

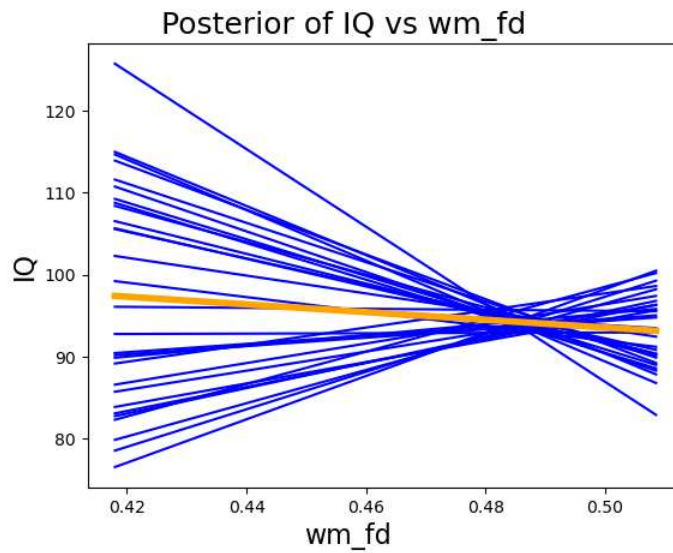


Figure 47 - Effect size of fibre density on IQ, blue depicts predictions by drawing from the posterior distribution, orange depicts mean of predictions